

This discussion paper is/has been under review for the journal Biogeosciences (BG).  
Please refer to the corresponding final paper in BG if available.

# Efficiency and adaptability of the benthic methane filter at Quepos Slide cold seeps, offshore Costa Rica

P. Steeb<sup>1</sup>, S. Krause<sup>1</sup>, P. Linke<sup>1</sup>, C. Hensen<sup>1</sup>, A. W. Dale<sup>1</sup>, M. Nuzzo<sup>2,\*</sup>, and T. Treude<sup>1</sup>

<sup>1</sup>GEOMAR Helmholtz Centre for Ocean Research Kiel, Wischhofstrasse 1–3, 24148 Kiel, Germany

<sup>2</sup>LNEG, Marine Geology Department, Alfragide, Portugal and Institute Dom Luiz, University of Lisbon, Lisbon, Portugal

\* now at: Integrated Geochemical Interpretation, Ltd., Bideford, UK

Received: 20 September 2014 – Accepted: 29 October 2014 – Published: 25 November 2014

Correspondence to: P. Steeb (psteeb@geomar.de) and T. Treude (ttreude@epss.ucla.edu)

Published by Copernicus Publications on behalf of the European Geosciences Union.

## Efficiency of the methane filter, Quepos Slide

P. Steeb et al.

[Title Page](#)

[Abstract](#)

[Introduction](#)

[Conclusions](#)

[References](#)

[Tables](#)

[Figures](#)



[Back](#)

[Close](#)

[Full Screen / Esc](#)

[Printer-friendly Version](#)

[Interactive Discussion](#)



## Abstract

Large amounts of methane are delivered by fluids through the erosive forearc of the convergent margin offshore Costa Rica and lead to the formation of cold seeps at the sediment surface. Besides mud extrusion, numerous cold seeps are created by landslides induced by seamount subduction or fluid migration along major faults. Most of the dissolved methane reaching the seafloor at cold seeps is oxidized within the benthic microbial methane filter by anaerobic oxidation of methane (AOM). Measurements of AOM and sulfate reduction as well as numerical modeling of porewater profiles revealed a highly active and efficient benthic methane filter at Quepos Slide site; a landslide on the continental slope between the Nicoya and Osa Peninsula. Integrated areal rates of AOM ranged from  $12.9 \pm 6.0$  to  $45.2 \pm 11.5 \text{ mmol m}^{-2} \text{ d}^{-1}$ , with only 1 to 2.5% of the upward methane flux being released into the water column.

Additionally, two parallel sediment cores from Quepos Slide were used for in vitro experiments in a recently developed **Sediment-Flow-Through** (SLOT) system to simulate an increased fluid and methane flux from the bottom of the sediment core. The benthic methane filter revealed a high adaptability whereby the methane oxidation efficiency responded to the increased fluid flow within 150–170 days. To our knowledge, this study provides the first estimation of the natural biogeochemical response of seep sediments to changes in fluid flow.

## 1 Introduction

Subduction zones represent large-scale systems of sediment and element recycling. Organic carbon accumulation at continental margins can lead to the formation of large methane reservoirs through its biological or thermogenic breakdown (Judd et al., 2002; Schmidt et al., 2005; Hensen and Wallmann, 2005; Crutchley et al., 2014). Produced methane gas may be transported upwards in solution by molecular diffusion or by

BGD

11, 16033–16083, 2014

## Efficiency of the methane filter, Quepos Slide

P. Steeb et al.

Title Page

Abstract

Introduction

Conclusions

References

Tables

Figures



Back

Close

Full Screen / Esc

Printer-friendly Version

Interactive Discussion



## Efficiency of the methane filter, Quepos Slide

P. Steeb et al.

Title Page

Abstract

Introduction

Conclusions

References

Tables

Figures



Back

Close

Full Screen / Esc

Printer-friendly Version

Interactive Discussion



ascending fluids mobilized by (i) sediment compaction or clay mineral dehydration (Hensen et al., 2004; Tryon et al., 2010; Crutchley et al., 2014) and (ii) formation of gas hydrates within the gas hydrates stability zone (GHSZ) (Torres et al., 2004; Burwicz et al., 2011; Wallmann et al., 2012). When the fluids are highly enriched in hydrocarbon gases, gas hydrates may precipitate depending on the pressure-temperature conditions (Hensen and Wallmann, 2005). Gas hydrates sometimes block fluid pathways (Tryon et al., 2002; Minami et al., 2012) and change the composition of fluids flowing through the GHSZ. Alternatively, dissociating gas hydrates can act as additional sources for methane and fluids (Kvenvolden, 2002), or dilute fluids when they dissolve (Hesse et al., 2000; Hensen et al., 2004).

The migration of methane-charged fluids towards the sediment–water interface creates so called “cold seeps” (Judd et al., 2002; Suess, 2010). Within the surface sediment, the majority of the methane is consumed by the anaerobic oxidation of methane (AOM) (Hinrichs and Boetius, 2002; Knittel and Boetius, 2009). AOM is coupled to sulfate reduction and produces dissolved bicarbonate and sulfide. The reaction is mediated by a consortia of anaerobic methanotrophic (ANME) archaea and sulfate-reducing bacteria (SRB) (Boetius et al., 2000). Recent studies propose that some ANME can reduce sulfate without the aid of SRB (Milucka et al., 2012). Additionally, the use of other electron acceptors such as Mn, Fe (Beal et al., 2009), or nitrate (Ettwig et al., 2010) is also possible. However, sulfate is the most abundant electron acceptor in seawater and AOM coupled to sulfate reduction is, to our knowledge, the by far most important anaerobic pathway for methane oxidation in marine settings (Reeburgh, 2007).

The sediment zone, in which methane and sulfate concentrations overlap, is termed the sulfate-methane transition zone (SMTZ). The depth of the SMTZ is dependent on (1) sulfate depletion resulting from organic matter degradation (Borowski et al., 1999), (2) sulfate supply by diffusion, bioirrigation and sulfide re-oxidation reactions (Dale et al., 2009) (3) the flux of methane from below the SMTZ (Borowski et al., 1996), and (4) the advective fluid flow rate (Treude et al., 2003; Orcutt et al., 2011). The

SMTZ can be located as deep as 160 m below the seafloor (m b.s.f.) at continental margins and sometimes even many hundreds of meters deep (Borowski et al., 1999). In coastal sediments, sulfate is consumed rapidly via organoclastic sulfate reduction fueled by an enhanced supply of organic matter and, subsequently, the SMTZ is often located closer to the sediment–water interface compared to sediments in greater water depths (Hinrichs and Boetius, 2002). At seepage sites, upwards advective flow of methane-rich fluid pushes the SMTZ closer to the surface, occasionally to only a few centimeters below the seafloor (cm b.s.f.) (Treude et al., 2003; Niemann et al., 2006; Krause et al., 2014). At the center of the Håkon Mosby Mud Volcano, advective fluid flow is so high that it inhibits sulfate penetration into the sediment (de Beer et al., 2006; Niemann et al., 2006), resulting in the absence of a SMTZ. The depth of the SMTZ determines, which chemolithotrophic seep organisms have access to the produced sulfide. The prevailing communities serve as indicators of seepage intensity. Sites covered by mats of sulfur bacteria (e.g. *Beggiatoa*) exhibit a very shallow SMTZ (few cm) compared to clam sites (e.g. *Calyptogena*) with SMTZ depth of ~5–10 cm, or even deeper SMTZ in tubeworm or *Solemya* habitats (Sahling et al., 2002; Levin, 2003; Treude et al., 2003; Mau et al., 2006; Fischer et al., 2012).

In this study, we present the first direct rate measurements of AOM and sulfate reduction for Quepos Slide, a submarine landslide on the Pacific coast off Costa Rica (Bohrmann et al., 2002; Karaca et al., 2012). A numerical model was developed to compare with the rate measurements and determine the magnitude of the fluid advection velocity. Because methane is an important greenhouse gas, it is not only our interest to quantify the efficiency of the benthic methane filter at steady state, but also the response of the filter to variable fluid flow conditions. To investigate the development of the geochemical gradients and dynamics under such conditions, as well the efficiency of the benthic microbial methane filter, we performed laboratory experiments with undisturbed seep sediments from Quepos Slide and exposed them to different flow conditions. For this, we used a newly developed **Sediment-Flow-**

## BGD

11, 16033–16083, 2014

### Efficiency of the methane filter, Quepos Slide

P. Steeb et al.

Title Page

Abstract

Introduction

Conclusions

References

Tables

Figures



Back

Close

Full Screen / Esc

Printer-friendly Version

Interactive Discussion



Through system referred to as SLOT (Steeb et al., 2014), which mimics natural fluid-flow regimes.

## 1.1 Geological setting

At the Mid-American Trench, the Cocos Plate in the north and Nazca Plate in the south are subducted below the Caribbean Plate at a velocity of  $8.8 \text{ cm yr}^{-1}$  (Syracuse and Abers, 2006). Here, seep features like mud volcanoes, mud diapirs, and pockmarks are very abundant. More than 100 seeps localities have been identified at the central Costa Rican Pacific Trench, on average one seep every 4 km Sahling et al., 2008). Recent high-resolution mapping revealed even greater seep density in this region (Kluesner et al., 2013). Between the Nicoya (north) and Osa Peninsula (south), seamounts from the Nasca Plate are subducted (Ranero and von Huene, 2000), resulting in slope failures and huge landslides or scarps (e. g., Jaco Scarp, BGR landslide, GEOMAR landslide; Harders et al., 2011; Ranero et al., 2008). Landslide-induced seeps are created by opening new structural and stratigraphical fluid pathways (Ranero et al., 2008; Mau et al., 2012) or by gas hydrate dissociation resulting from altered pressure and temperature conditions.

Fluids and related methane fluxes can vary both spatially and temporally as well as in origin, composition, and flow velocity. Temporal variations can be caused by gas hydrate formation and dissociation (Hesse et al., 2000; Tryon et al., 2002; Hensen et al., 2004; Minami et al., 2012) or triggered by earthquakes, which are frequent in this active subduction zone (Tryon et al., 2002; Hensen et al., 2004; Aiello, 2005; Henrys et al., 2006; Mau et al., 2007; Fischer et al., 2013).

Well-known examples exhibiting such dynamics are the twin mounds “Mound 11” and “Mound 12”, located at 1000 m water depth, halfway between the Nicoya and Osa Peninsulas. Both mounds are located at the same fault zone, although they differ in fluid flow advection intensity (Hensen et al., 2004; Linke et al., 2005; Karaca et al., 2010; Krause et al., 2014), fluid origin (Hensen et al., 2004; Han et al., 2004; Schmidt et al., 2005), and microbial activity (Krause et al., 2014). In the last 50 kyr both mounds

### Efficiency of the methane filter, Quepos Slide

P. Steeb et al.

Title Page

Abstract

Introduction

Conclusions

References

Tables

Figures



Back

Close

Full Screen / Esc

Printer-friendly Version

Interactive Discussion



have displayed individual active phases interrupted by phases of inactivity (Kutterolf et al., 2008). In contrast to this long term variability, Füre et al. (2010) observed a two month seepage event at Mound 11 with flow rates that varied four-fold (from 5 to 20 cm yr<sup>-1</sup>). Events like this affect the efficiency of the benthic microbial methane filter and result in increased methane concentrations in the water column. Slow adaptation to increased methane supply may explain elevated methane concentrations in the water column offshore Costa Rica made by Mau et al. (2007) in 2003, presumably caused by an earthquake earlier that year.

The research area of the present study, the Quepos Slide, is located south of the twin Mounds 11 and 12. This landslide is approximately 9.5 km wide and 8 km long (Harders, 2011). The translational slide has a headwall 160 m in height and the slide head is located at ~ 400 m water depth in the Eastern Pacific oxygen minimum zone (OMZ; between 250 and 550 m water depth; Bohrmann et al., 2002). Four tongues of the landslide can be identified, reaching down to ~ 800 water depth, indicating three subsequent events following the initial slide (Bohrmann et al., 2002; Harders et al., 2011). The Quepos Slide was most likely caused by seamount subduction (Harders et al., 2011). Along the toe, fluids and gas can migrate from hydrates inside the GHSZ. Chemosynthetic organisms are abundant, with bacterial mats present throughout, while authigenic carbonates and clams can be found at deeper areas and at the toe of the slide (Bohrmann et al., 2002). Directly below the headwall, the sediments are covered by sulfur bacteria mats (Bohrmann et al., 2002; Sahling et al., 2008; Karaca et al., 2012). Empirical models show that vertical fluid flow at Quepos Slide varies between 1 and 40 cm yr<sup>-1</sup> and AOM rates vary between 1.5 and 42.1 mmol m<sup>-2</sup> d<sup>-1</sup> (Karaca et al., 2012). According to that model, 53 % (~ 316 × 10<sup>3</sup> molyr<sup>-1</sup>) of the methane is oxidized by the highly active benthic microbial methane filter, while 47 % (280 × 10<sup>3</sup> molyr<sup>-1</sup>) is released into the water column. Elevated methane concentrations of 72 nmol L<sup>-1</sup> was observed in the seawater directly above the slide head (Bohrmann et al., 2002).

## Efficiency of the methane filter, Quepos Slide

P. Steeb et al.

[Title Page](#)[Abstract](#)[Introduction](#)[Conclusions](#)[References](#)[Tables](#)[Figures](#)[Back](#)[Close](#)[Full Screen / Esc](#)[Printer-friendly Version](#)[Interactive Discussion](#)

## 2 Methods

Surface sediments from Quepos Slide were obtained by a video-guided multi-corer (TV-MUC) during the GEOMAR research cruise SO206 on the German research vessel "SONNE". Two sites (SO206-29 MUC, SO206-31 MUC) from the headwall of Quepos Slide, both covered by sulfur bacteria mats, were sampled (Table 1). All subsampling procedures were performed on board at 4 °C immediately after obtaining the sediments. Three replicate cores of each TV-MUC were used for (1) porewater analyses, (2) ex situ AOM and sulfate reduction rate assays, and (3) methane concentration determination. Additionally, two replicate cores of SO206-31 (MUC) were sub-sampled for laboratory experiments (SLOT-system, see below).

### 2.1 Porewater measurement (ex situ)

Porewater of the ex situ samples was extracted by a pressure-filtration system and filtered (argon 3–4 bar, 0.2 µm regenerated cellulose filters, Krause et al., 2014). Total alkalinity (TA) was analyzed onboard via titration (Ivanenkov and Lyakhin, 1978). Sulfide was determined photometrically by using the methylene blue method (Cline, 1969). Sub-samples for the determination of sulfate, chloride, and bromide were frozen and analyzed onshore by ion chromatography (Compact IC 761). Further porewater sampling and analytical procedures are described in detail by Krause et al. (2013).

### 2.2 Methane (ex situ)

For methane determination, 10 cm<sup>3</sup> of sediment was transferred to glass vials filled with 10 mL 10% KCl for poisoning and headspace equilibration. Methane concentrations were measured onboard using a Shimadzu GC14A gas chromatograph fitted with a Restek® Alumina Bond capillary column and operated with nitrogen as carrier gas.

## Efficiency of the methane filter, Quepos Slide

P. Steeb et al.

Title Page

Abstract

Introduction

Conclusions

References

Tables

Figures



Back

Close

Full Screen / Esc

Printer-friendly Version

Interactive Discussion



## 2.3 Microbial rate measurement (ex situ)

Ex situ turnover rates of sulfate reduction and AOM were determined with radiotracer techniques. For both sulfate reduction and AOM, three replicate polycarbonate tubes (26 mm inner diameter, 250 mm length) were sub-sampled from one TV-MUC core and incubated by whole core incubation (Jørgensen 1978). Additional bulk sediment was sampled to produce controls. Fifteen  $\mu\text{L}$   $^{14}\text{CH}_4$  (1–2 kBq dissolved in anoxic, sterile water; specific activity 22.28 GBq mmol<sup>-1</sup>), and 6  $\mu\text{L}$   $^{35}\text{SO}_4^{2-}$  (200 kBq dissolved in water; specific activity 37 TBq mmol<sup>-1</sup>), was injected into the AOM and sulfate reduction cores, respectively, at a vertical resolution of 1 cm; the cores were then incubated for 24 h in the dark at in situ temperature (8 °C). After incubation, the sediment cores were sliced in 1 cm intervals and transferred to 20 mL NaOH (2.5 % w/v, 40 mL glas vials with rubber stopper) for AOM, and 20 mL zinc acetate (20 % w/v, 50 mL plastic vials) for sulfate reduction determinations. Controls samples (five each), were first transferred to the respective chemicals before tracer was added (see above). AOM was determined according to Treude et al. (2005) (GC and Combustion) and Joye et al. (2004) ( $^{14}\text{CO}_2$  trapping). Sulfate reduction was determined using the cold chromium distillation method after Kallmeyer et al. (2004).

## 2.4 Numerical model

Porewater profiles were simulated using a one-dimensional transport reaction model, previously used and described by Krause et al. (2013), to determine the flow velocity of the fluid and the rate of AOM. Carbonate precipitation was implemented in the model (Krause et al., 2013) but was not used in the present study for simplicity, since carbonate precipitation does not affect the efficiency of the microbial benthic methane filter within the studied time scales (several month to years). Because the sampling sites were located above the GHSZ (Wallmann et al., 2012), dissolved methane concentrations at the lower boundary were calculated from the equilibrium concentration with free gas

**BGD**

11, 16033–16083, 2014

### Efficiency of the methane filter, Quepos Slide

P. Steeb et al.

Title Page

Abstract

Introduction

Conclusions

References

Tables

Figures



Back

Close

Full Screen / Esc

Printer-friendly Version

Interactive Discussion



Tishchenko et al., 2005). Table 4 provides an overview of other boundary conditions as well as fitted, measured, and calculated parameters of the model.

## 2.5 Sediment-flow-through system

The response of the sediment to changes in fluid and methane fluxes was studied using a newly-developed **Sediment-Flow-Through** (SLOT)-system (Steeb et al., 2014), which mimics natural flow conditions with diffusive supply of sulfate at the sediment surface and advective methane supply at the bottom of the core. The system enables continuous monitoring of geochemical gradients inside the sediment as well as in the in- and outflow and allows the development of the geochemical gradients and SMTZ to be observed. The efficiency of the benthic microbial methane filter during the transient periods can be calculated from the measured input and output fluxes (see below). For SLOT experiments, two replicate multicorer cores from station SO206-31 (MUC) were sub-sampled with specific SLOT liners (Steeb et al., 2014). Liners were closed with rubber stoppers, and sealed with electrical tape for transport. At GEOMAR, filters (glass fiber, Whatman GF/F) were applied at the bottom of the sediment core and at the lower and upper cap, as previously described (Steeb et al., 2014).

Two different seawater media were applied: one medium, resembling seawater, was amended to natural sulfate concentrations ( $28 \text{ mmol L}^{-1}$ ). The added sulfate penetrated the sediment by diffusion. The other medium, resembling sulfate-free seepage fluid, carried dissolved methane ( $965 \pm 180 \mu\text{mol L}^{-1}$ ) upwards into the bottom of the core by advection. Both media were based on the sulfate reducer medium developed by Widdel and Bak (2006). In the “seepage” medium,  $\text{MgSO}_4$  was replaced by  $\text{MgCl}$ . Both media were kept anoxic, and contained resazurin as oxygen indicator (Visser et al., 1990), with a pH adjusted to 7.5 and a salinity of 35 PSU. Bromide served as an inert tracer for the upward migration and was present only in the methane-enriched seepage medium ( $800 \mu\text{mol L}^{-1}$ ). Hence, the depth where bromide and sulfate concentrations overlapped was interpreted as the SMTZ. We therefore used the sulfate-bromide transition zone (SBTZ) as a proxy for the SMTZ and defined it as the zone with the steepest  $\text{SO}_4^{2-}$

BGD

11, 16033–16083, 2014

### Efficiency of the methane filter, Quepos Slide

P. Steeb et al.

Title Page

Abstract

Introduction

Conclusions

References

Tables

Figures



Back

Close

Full Screen / Esc

Printer-friendly Version

Interactive Discussion



and  $\text{Br}^-$  gradients. Medium composition and the gas headspace composition of the reservoirs are summarized in Table 2.

SLOT experiments were performed with two sediment cores under different flow regimes. One core was exposed to a relatively moderate advective fluid flow velocity (10.6  $\text{cm yr}^{-1}$ ), here further referred as the **low flow core (LFC)**, whereas the other core was exposed to a 10-fold higher advective fluid flow velocity (106.3  $\text{cm yr}^{-1}$ ), further referred as the **high flow core (HFC)**. The moderate fluid flow velocities were on the same order as those determined by the numerical model (see Results). The high flow velocities were more than twice of those previously reported for Quepos Slide (40  $\text{cm yr}^{-1}$ ; Karaca et al., 2012) and were employed to observe the sediment response under extreme fluid flow. Similar or even higher (up to 200  $\text{cm yr}^{-1}$ ) advective flow velocities have been reported for seeps within the same region (Hensen et al., 2004; Linke et al., 2005; Karaca et al., 2010; Krause et al., 2014). The applied fluid flow velocities were strong enough to observe considerable changes within the time frame of one year yet weak enough to avoid sulfate penetration to less than one cm.

In the initial preparation phase of the experiment (40 days), the outflow of the system was located at the bottom of the core and only methane-free seawater medium was pumped from top to bottom. This procedure was applied to establish a homogeneous sulfate distribution and anoxic conditions throughout the entire sediment column without disturbing the sediment fabric. In the subsequent first experimental phase, the outflow was mounted at the top of the core and seawater medium was delivered to the overlying seawater at a pump rate of 20  $\mu\text{L min}^{-1}$ . From this point, sulfate was transported into the sediment core solely via diffusion. From the bottom, the seepage medium was supplied at 0.5  $\mu\text{L min}^{-1}$  (LFC) and 5  $\mu\text{L min}^{-1}$  (HFC) with an average inflow methane concentration of  $965 \pm 180 \mu\text{mol L}^{-1}$ . Based on the pump rate, methane concentration, and surface area of the sediment, a methane flux of 0.28 and 2.81  $\text{mmol m}^{-2} \text{d}^{-1}$  was calculated for the LFC and HFC core, respectively. These methane concentrations were lower than those potentially encountered under in situ conditions because the cores were not pressurized, resulting in lower methane fluxes

## BGD

11, 16033–16083, 2014

### Efficiency of the methane filter, Quepos Slide

P. Steeb et al.

Title Page

Abstract

Introduction

Conclusions

References

Tables

Figures



Back

Close

Full Screen / Esc

Printer-friendly Version

Interactive Discussion



(after Tishchenko et al., 2005; Karaca et al., 2012). After 260 days the first experimental phase ended and the pump rates were increased from low to high flow velocities for the LFC, and vice versa for the HFC. This switch marked the beginning of the second and final experimental phase to study the response of AOM to rapid changes in the flow regime. After 316 days, the experiment was terminated and the cores were sliced and sub-sampled for further analyses (see below).

Methane emission from the sediment was calculated by multiplying the out-flow methane concentrations ( $\text{CH}_{4\text{out}}$ ) with the dilution factor (DF; 41 and 5 for LFC and HFC, respectively) and the fluid flow ( $v$ ; 10.6 and 106.3  $\text{cm yr}^{-1}$  for LFC and HFC, respectively) according to Eq. (1).

$$\text{CH}_{4\text{efflux}} [\text{mmol m}^{-2} \text{d}^{-1}] = v [\text{cm yr}^{-1}] \cdot \text{CH}_{4\text{out}} [\text{mmol cm}^{-3}] \cdot \text{DF} \cdot \frac{10\,000}{365.25} \quad (1)$$

Areal AOM rates ( $\text{AOM}_{\text{areal}}$ ) were calculated from the difference between in- ( $\text{CH}_{4\text{in}}$ ) and outflow ( $\text{CH}_{4\text{out}}$ ) methane concentrations before (258 days) and after (316 days) fluid flow velocity change according to Eq. (2),

$$\text{AOM}_{\text{areal}} [\text{mmol m}^{-2} \text{d}^{-1}] = \left( \frac{\text{CH}_{4\text{in}} [\text{mmol cm}^{-3}] - \text{CH}_{4\text{out}} [\text{mmol cm}^{-3}] \cdot \text{DF}}{\text{HRT} [\text{d}]} \right) \cdot \frac{10\,000}{\text{SLOT}_{\text{base}} [\text{cm}^2]} \quad (2)$$

with  $\text{SLOT}_{\text{base}}$  for the base area of the SLOT-cores and DF for the dilution factor in the overlying water, resulting from the different pump rates for the “seepage” and “seawater” media and their mixing in the overlying water. HRT stands for the hydrological residence time, the average time of the seepage medium to flow through the sediment column and was calculated by dividing the porewater volume by the flow rate.

**Efficiency of the methane filter, Quepos Slide**

P. Steeb et al.

Title Page

Abstract

Introduction

Conclusions

References

Tables

Figures



Back

Close

Full Screen / Esc

Printer-friendly Version

Interactive Discussion



## 2.6 Geochemical parameters during SLOT experimentation

During the SLOT experiments, geochemical parameters were measured in 1 cm depth intervals throughout the sediment core. In addition, concentrations in the in- and out-flowing fluids were monitored. Sulfide concentrations, pH, and redox potential were measured with microsensors (sulfide needle sensor, H<sub>2</sub>S-N, tip diameter 0.8 mm, Unisense; pH, MI 411 B, Gauge 20, Microelectrodes Inc.; redox potential needle sensors, MI-800, Gauge 25, Microelectrodes Inc.). Porewater samples (1.5–2 mL) for the determination of sulfate, bromide, and total alkalinity were obtained from each depth in the sediment using pre-installed rhizones (CSS-F, length 5 cm, diameter 2.5 mm, pore size 0.2 μm, Rhizosphere<sup>®</sup>). The in- and outflow of both cores were sampled with glass syringes for the determination of sulfate, bromide, total alkalinity and methane concentration. All sampling and measurement proceedings for the experiment are described in detail by Steeb et al. (2014).

## 2.7 Experiment termination and final sampling

At the end of the experiment, 1.5 mL porewater from each depth was sampled for determinations of sulfide (0.5 mL), sulfate and bromide (1.0 mL) as well as total alkalinity (0.5 mL), and analyzed after the same methods as the ex situ porewater (see Sect. 2.1).

After the final porewater sampling, sediment sub-samples were taken from each SLOT core. Two sub-cores (polycarbonate, length 260 mm, inner diameter 26 mm) were collected from each SLOT core for radiotracer determinations of AOM and sulfate reduction, and treated according to the protocols mentioned above. For the determination of methane concentrations, each SLOT core was sampled in 1 cm intervals (2 cm<sup>3</sup> volume sub-samples) using cut-off syringes (3 mL, PE). The sediment samples were transferred into glass vials (13 mL) with 5 mL 2.5 % w/v NaOH. Vials were closed with butyl rubber stoppers and shaken directly after sampling. Methane was analyzed by gas chromatography (Hewlett Packard Series II) with a packed column

### Efficiency of the methane filter, Quepos Slide

P. Steeb et al.

Title Page

Abstract

Introduction

Conclusions

References

Tables

Figures



Back

Close

Full Screen / Esc

Printer-friendly Version

Interactive Discussion



(Haye SepT, 6 ft, 3.1 mm inner diameter, 100/120 mesh, Resteck, carrier gas: He 20 mL min<sup>-1</sup>, combustion gas: synthetic air 240 mL min<sup>-1</sup>, H<sub>2</sub> 20 mL min<sup>-1</sup>).

The remaining sediment of each SLOT core was sampled in 2 cm depth intervals. For porosity measurements, approximately 2 cm<sup>3</sup> samples were obtained using cut-off syringes (3 mL, PE), transferred to pre-weighed vials, and weighed, before and after the sample was freeze-dried. Porosity was then calculated by the difference in weight (Dalsgaard et al., 2000). Sub-samples of the dried sediment were used to determine total carbon (TC), total nitrogen (TN), total sulfur (TS) and total organic carbon (TOC) of the solid phase. TC, TN, TS, and TOC were analyzed using a CARLO ERBA Elemental Analyzer NA 1500. For TOC determination, inorganic carbon was removed by adding hydrochloric acid. Total inorganic carbon (TIC) was calculated from the difference between TC and TOC. All solid phase analyses were carried out in duplicates.

Further details on the SLOT sampling procedure and analytical procedures are described in Steeb et al. (2014).

## 3 Results

### 3.1 Ex situ profiles

Both MUC cores (SO206-29 MUC and SO206-31 MUC) were sampled at ~ 400 m water depth from sediments covered with sulfur bacteria mats, which are indicative for high methane fluxes (Torres et al., 2002; Treude et al., 2003).

At station SO-206-29 (MUC), sulfate decreased from 28 mmolL<sup>-1</sup> at the sediment surface to zero at the bottom of the core (26 cm below sea floor; cm b.s.f.) (Fig. 1a). Conversely, methane concentrations were low (0.0–0.1 mmolL<sup>-1</sup>) in the upper 15 cm b.s.f. and increased below this zone to a maximum of 2.4 mmolL<sup>-1</sup> at the bottom (Fig. 1a). Accordingly, the SMTZ was located at approximately 17.5 cm b.s.f. Two maxima in sulfate reduction rates were identified in one of the replicate cores at the top (up to 1821 nmolcm<sup>-3</sup>d<sup>-1</sup>) and between 12.5 and 22.5 cm b.s.f. (up

BGD

11, 16033–16083, 2014

## Efficiency of the methane filter, Quepos Slide

P. Steeb et al.

Title Page

Abstract

Introduction

Conclusions

References

Tables

Figures



Back

Close

Full Screen / Esc

Printer-friendly Version

Interactive Discussion



## Efficiency of the methane filter, Quepos Slide

P. Steeb et al.

Title Page

Abstract

Introduction

Conclusions

References

Tables

Figures



Back

Close

Full Screen / Esc

Printer-friendly Version

Interactive Discussion



to  $879 \text{ nmol cm}^{-3} \text{ d}^{-1}$ ) (Fig. 1b). AOM coincided with the second sulfate reduction maximum and reached rates up to  $569 \text{ nmol cm}^{-3} \text{ d}^{-1}$  (Fig. 1c). Sulfide and total alkalinity (TA) increased from the top ( $0.0 \text{ mmol L}^{-1}$  and  $2.5 \text{ meq L}^{-1}$ , respectively) to a maximum within the SMTZ ( $7.9 \text{ mmol L}^{-1}$  and  $23.4 \text{ meq L}^{-1}$ , respectively, at 17.5 cm sediment depth), (Fig. 1d). Areal turnover rates of methane and sulfate integrated over the entire sediment depth of 26 cm were similar for AOM (on average  $12.87 \pm 5.98 \text{ mmol m}^{-2} \text{ d}^{-1}$ ) and sulfate reduction (on average  $13.38 \pm \text{SD } 13.61 \text{ mmol m}^{-2} \text{ d}^{-1}$ ) with a ratio of 0.96 (AOM: sulfate reduction), respectively.

The steady state model resulted in a fluid flow of  $7 \text{ cm yr}^{-1}$  and an areal AOM rate of  $11.34 \text{ mmol m}^{-2} \text{ yr}^{-1}$  (Table 4). In total, around 92 % of the delivered methane was oxidized by AOM and  $\sim 8\%$  was released to the seawater. Fitted porewater profiles and AOM rates are shown in Fig. 1.

In the second core, SO206-31 (MUC), sulfate decreased to  $0 \text{ mmol L}^{-1}$  within the first 15 cm sediment depth and considerable methane concentrations ( $> 3.4 \text{ mmol L}^{-1}$ ) were observed at 5 cm b.s.f. (Fig. 2a). The observed maximum methane concentration was  $10.2 \text{ mmol L}^{-1}$  (20.5 cm b.s.f.). Accordingly, the SMTZ was located at approximately 5–15 cm b.s.f. Sulfate reduction and AOM occurred between 0 and 12.5 cm b.s.f. with a sulfate reduction maximum ( $12052 \text{ nmol cm}^{-3} \text{ d}^{-1}$ ) at the top of the SMTZ ( $\sim 2.5 \text{ cm b.s.f.}$ ) and an AOM maximum ( $1400 \text{ nmol cm}^{-3} \text{ d}^{-1}$ ) in the upper part of the SMTZ (5.5 cm b.s.f.) (Fig. 2b and c). Highest sulfide and TA concentrations were measured within the SMTZ between 10 and 15 cm b.s.f. ( $8.6 \text{ mmol L}^{-1}$  and  $24.1 \text{ meq L}^{-1}$ , respectively) (Fig. 2d). Areal sulfate reduction rates integrated over the entire sediment depth of 25 cm ( $218.90 \pm 159.80 \text{ mmol m}^{-2} \text{ d}^{-1}$ ) were around 5 times (AOM: SR = 0.21) higher compared to the areal rates of AOM ( $45.15 \pm 11.48 \text{ mmol m}^{-2} \text{ d}^{-1}$ ) integrated over of the same depth.

Replicate cores for porewater and rate analyses from SO206-31 showed a difference in depth of the SMTZ. Based on this lateral heterogeneity, two different fits were applied for the numerical model; one for the porewater (pw-fit) and another where the model simulated instead the rates, which required higher fluid advection (hf-

fit). The pw-fit with  $7 \text{ cm yr}^{-1}$  fluid flow showed an efficient benthic filter which oxidized all delivered methane ( $9.09 \text{ mmol m}^{-2} \text{ d}^{-1}$ ). The hf-fit ( $29 \text{ cm yr}^{-1}$ ) had an AOM rate of  $41.69 \text{ mmol m}^{-2} \text{ d}^{-1}$  and oxidized around 93% of the delivered methane ( $45.09 \text{ mmol m}^{-2} \text{ d}^{-1}$ ). Model results are shown in Fig. 2 and summarized in Table 4.

## 5 3.2 SLOT incubation experiments

For the SLOT-Incubations, two replicate cores from SO206-31 (MUC) were used.

### 3.2.1 Evolution of biogeochemical parameters during the main phase of the experiment (0–260 days)

\*

#### 10 The low fluid flow regime core

In the low flow regime core (LFC) incubations, **bromide** concentration, which was used as a tracer to track the seepage medium, was always very low and near detection limit ( $20 \mu\text{mol L}^{-1}$ ). Values increased only weakly in the lowest 5 cm of the core, reaching a maximum of  $45 \mu\text{mol L}^{-1}$  after 49 days (Fig. 3d). **Sulfate**, which was delivered from the top by diffusion, decreased only slightly at the bottom of the core ( $27.2 \text{ mmol L}^{-1}$ ) due to a slow advection of methane-enriched seepage medium. This was in accordance with the small increase in bromide (up to  $\sim 45 \mu\text{mol L}^{-1}$ ). After 105 days, sulfate levels stabilized around  $26 \text{ mmol L}^{-1}$  at the bottom of the core and did not further decrease during the low flow phase.

20 In the first 105 days, **sulfide** concentrations of the LFC core varied between 23 and  $300 \mu\text{mol L}^{-1}$  over depth with a maximum between 9 and 11 cm (Fig. 3b, e, and h). After 171 days, a sulfide peak ( $920 \mu\text{mol L}^{-1}$ , Fig. 3k) occurred at 0.26 cm sediment depth, while no sulfide was detected in the overlying water. Below the peak, sulfide varied between 300 and  $500 \mu\text{mol L}^{-1}$ . Thirty days later (201 day runtime), maximum

## Efficiency of the methane filter, Quepos Slide

P. Steeb et al.

Title Page

Abstract

Introduction

Conclusions

References

Tables

Figures



Back

Close

Full Screen / Esc

Printer-friendly Version

Interactive Discussion



sulfide concentrations of up to  $230 \mu\text{molL}^{-1}$  were observed between 1.5 and 10.7 cm sediment depth (Fig. 3n). After 258 days, directly before changing from low to high fluid flow, maximum sulfide concentrations were  $115 \mu\text{molL}^{-1}$  at 4.5–5.5 cm b.s.f. (Fig. 3q) and decreased to a minimum of  $36 \mu\text{molL}^{-1}$  near the sediment–water interface.

**Total alkalinity (TA)** was predominantly lower inside the cores than in the media ( $30 \text{ meqL}^{-1}$ ). During the LFC incubation, TA continuously decreased over the time from  $\sim 30$  to  $\sim 24 \text{ meqL}^{-1}$  below  $\sim 9$  cm (Fig. 3b, e, h, and k). After 171 days, TA varied between 28.7 and  $21.7 \text{ meqL}^{-1}$ . Directly before the change of fluid flow (258 days), TA increased from the top ( $23.3 \text{ meqL}^{-1}$ ) to the bottom ( $26.7 \text{ meqL}^{-1}$ ; Fig. 3q).

Initial **redox potential** of the LFC was  $-50$  mV at the top and around  $-150$  mV below 2 cm sediment depth (Fig. 3c). After 49 days, the redox potential was more negative ( $-130$  mV at top and between  $-160$  to  $-270$  mV below, Fig. 3f); after 105 days, the redox potential increased to  $-80$  mV at the top (Fig. 3i). Between 171 and 202 day runtime, the overlying water of the core showed a pink color caused by the oxygen indicator resazurin. At the same time, the redox potential was positive (between 150 and 100 mV) at the sediment water interface (Fig. 3l and o), probably as a result of oxygen intrusion. Nevertheless, free oxygen should result in a redox potential  $> 350$  mV (Schulz, 2000). We therefore assume that oxygen was only temporally available and rapidly consumed. Deeper inside the sediment, redox potential reached values between  $-200$  and  $-400$  mV (Fig. 3l and o).

Directly before changing the fluid flow (258 days), the redox potential of the LFC was  $-100$  mV in the overlying water and around  $-200$  mV inside the sediment (Fig. 3r).

After 171 day runtime, **pH** was highest at the sediment–water interface (8.2, Fig. 3l) and around 7.6 deeper in the sediment. Final pH before fluid flow swapping (258 days) decreased from 7.6 at the top to 7.1 at the bottom of the core (Fig. 3r).

**Methane** concentrations in the out-flow of the LFC started at  $1.5 \mu\text{molL}^{-1}$  (29 days) and increased to  $2.5 \mu\text{molL}^{-1}$  after 105 days before decreasing again to  $0.9 \mu\text{molL}^{-1}$  after 258 days (Fig. 5). Calculated methane efflux followed the methane concentration trend. The LFC methane efflux was between  $0.011$  and  $0.030 \text{ mmolm}^{-2} \text{ d}^{-1}$ . AOM

## Efficiency of the methane filter, Quepos Slide

P. Steeb et al.

Title Page

Abstract

Introduction

Conclusions

References

Tables

Figures



Back

Close

Full Screen / Esc

Printer-friendly Version

Interactive Discussion





bottom (Fig. 4b, e, and h). After 171 days, this distribution reversed with TA increasing from the top of the core to the bottom, from 21–26 to 24–27 meqL<sup>-1</sup> (Fig. 4k).

The **redox potential** of the HFC core was, similar to the LFC core, highest at the sediment–water interface and in the overlying water and lowest at larger depths of the core. Initially (21 days), redox potential was –85 mV at the sediment water interface and between –100 and –150 mV in the sediment (Fig. 4c). Over time, the redox potential in the sediment became more negative, reaching a value down to –385 mV after 105 days (Fig. 4i and l). Between 105 and 202 day runtime, the overlying water turned pink and showed a redox potential ranging from 100 to 200 mV (Fig. 4q), indicating oxygen contamination in the core. Directly before the change in fluid flow, the redox potential returned to negative values with –120 mV in the overlying water and around –200 mV in remaining core (Fig. 4r).

Similar to the LFC core, the **pH** was highest at the sediment–water interface and lower inside the sediment (8.1–7.8 after 171 days and 8.0–7.4 after 202 days; Fig. 4l and o). Directly before the fluid flow change (258 days), pH decreased to 7.6 at the sediment water interface and to 7.1–7.3 inside the sediment (Fig. 4r).

**Methane** concentration in the HFC outflow was initially (21 days) 7.5 μmolL<sup>-1</sup> and then decreased to 1.7 μmolL<sup>-1</sup> during the following 200 days. After 258 days runtime, methane concentration in the outflow increased again to 2.8 μmolL<sup>-1</sup>. Efflux of the HFC ranged from 0.025 up to 0.109 mmolm<sup>-2</sup>d<sup>-1</sup>. Corresponding calculated AOM rates were 3.114 mmolm<sup>-2</sup>d<sup>-1</sup> directly before changing the flow rate (258 days).

### 3.2.2 Biogeochemical responses after changing the fluid flow regime (260–350 day runtime)

After 260 days, the fluid flow in the cores was swapped from low to high and vice versa.

\*

**BGD**

11, 16033–16083, 2014

## Efficiency of the methane filter, Quepos Slide

P. Steeb et al.

Title Page

Abstract

Introduction

Conclusions

References

Tables

Figures

⏪

⏩

◀

▶

Back

Close

Full Screen / Esc

Printer-friendly Version

Interactive Discussion



## New high flow regime core

In the new high flow regime core (NHFC, former LFC) sulfate and bromide concentrations did not change considerably over the entire runtime (350 days). TA remained constant at  $25 \text{ meqL}^{-1}$  (Fig. 3t). Sulfide concentrations were highest at 0.3 cm sediment depth ( $1230 \text{ } \mu\text{molL}^{-1}$ ) and first decreased steeply followed by a more steady increase (below 3 cm) with the exception of a second maximum ( $625 \text{ } \mu\text{molL}^{-1}$ ) at 5 cm. At the bottom of the core, a sulfide concentration of max  $75 \text{ } \mu\text{molL}^{-1}$  was reached. Redox potential was positive (31 mV) in the overlying water and between  $-280$  and  $-330$  mV within the sediment (Fig. 3u). The pH decreased from 8.5 to 7.5 between the sediment–water interface and the bottom of the core.

Methane concentration of the outflow increased considerably from 0.9 to  $11.6 \text{ } \mu\text{molL}^{-1}$  after 316 day run time. Calculated methane effluxes were  $0.165 \text{ mmol m}^{-2} \text{ d}^{-1}$  and corresponding AOM rates were  $2.970 \text{ mmol m}^{-2} \text{ d}^{-1}$ .

## New low flow regime core

In the new low flow regime core (NLFC; former HFC), sulfate penetrated deeper and bromide ascended less into the sediment, as compared to the profile prior to fluid flow change (Fig. 4s). Sulfide concentrations remained low, between  $50$  and  $80 \text{ } \mu\text{molL}^{-1}$ , and TA varied between  $23$  and  $25 \text{ meqL}^{-1}$  (Fig. 4t). Redox potential was positive ( $150$  mV) at the sediment water interface and the upper sediment (Fig. 4u). Below 2 cm sediment depth, redox decreased to values between  $-200$  and  $-400$  mV. The pH profile decreased from 8.05 in the overlying water and at the sediment–water interface down to 7.55 below 6 cm sediment depth.

Methane concentrations in the outflow declined from  $2.8$  to  $0.7 \text{ } \mu\text{molL}^{-1}$ . Calculated methane effluxes were  $0.009 \text{ mmol m}^{-2} \text{ d}^{-1}$  with a corresponding AOM rate of  $0.306 \text{ mmol m}^{-2} \text{ d}^{-1}$ .

## Efficiency of the methane filter, Quepos Slide

P. Steeb et al.

Title Page

Abstract

Introduction

Conclusions

References

Tables

Figures



Back

Close

Full Screen / Esc

Printer-friendly Version

Interactive Discussion



### 3.2.3 Biogeochemical parameters after experiment termination

After 350 day runtime, the experiment was terminated, porewater was sampled, and the sediment sub-sampled for further analyses. In both cores, methane concentrations determined after experiment termination (around  $2.5 \mu\text{molL}^{-1}$ ) were only a minor fraction of the original inflow concentration ( $965 \mu\text{molL}^{-1}$ ), which was attributed to methane losses during porewater extraction using rhizones directly before sediment sampling (Steeb et al., 2014). In the NHFC (= former LFC) methane concentrations varied between 2 and  $4 \mu\text{molL}^{-1}$  with a slight increase towards the bottom of the core (Fig. 6a). Sulfate concentrations decreased slightly from  $29.5 \text{ mmolL}^{-1}$  at the top to  $26.2 \text{ mmolL}^{-1}$  at the bottom of the core (Fig. 6b). Sulfide increased from  $50 \text{ mmolL}^{-1}$  at the sediment surface (0.3 cm) to a maximum of  $125 \mu\text{molL}^{-1}$  at 6 cm and decreased to  $80 \mu\text{molL}^{-1}$  at the bottom of the core (Fig. 6c). AOM rates of the NHFC determined by radiotracer techniques showed highest values between 4 to 10 cm sediment depth ( $0.50\text{--}0.91 \text{ nmolcm}^{-3} \text{ d}^{-1}$ ) and, in addition, increased from top ( $0.10 \text{ nmolcm}^{-3} \text{ d}^{-1}$ ) to bottom ( $0.33 \text{ nmolcm}^{-3} \text{ d}^{-1}$ ). Areal turnover rates of methane and sulfate integrated over the entire sediment core (0–15 cm) were  $0.043$  and  $2.31 \text{ mmolm}^{-2} \text{ d}^{-1}$  for AOM and sulfate reduction, respectively.

In the NLFC (= former HFC), methane concentrations remained consistently low at around  $2\text{--}4 \mu\text{molL}^{-1}$  (Fig. 7a). Sulfate was between  $27$  and  $28.5 \text{ mmolL}^{-1}$  within the upper first 6 cm and then decreased to  $10 \text{ mmolL}^{-1}$  below this depth (Fig. 7b). Consistent with the steepest decrease in sulfate, sulfide increased to a maximum of  $42 \mu\text{molL}^{-1}$ . Highest AOM rates determined with radiotracer techniques were detected between 5 and 11 cm ( $0.4\text{--}1 \text{ nmolcm}^{-3} \text{ d}^{-1}$ , Fig. 7a). Sulfate reduction rates ranged from  $16.95$  to  $27.71 \text{ nmolcm}^{-3} \text{ d}^{-1}$  in the upper sediment (0–6 cm depth) and decreased to  $7.96 \text{ nmolcm}^{-3} \text{ d}^{-1}$  at the bottom, which corresponded to a simultaneous decrease in sulfate at the bottom of the core (Fig. 6a). Areal rates integrated over the entire sediment depth (14 cm) were  $0.042$  and  $2.494 \text{ mmolm}^{-2} \text{ d}^{-1}$  for AOM and sulfate reduction, respectively.

The TC contents were similar in both, the NHFC and NLFC core, and varied between 4.97 and 6.05 dry wt% (Figs. 8a, 9a). A carbon peak (6.05 dry wt%, 7 cm sediment depth) resulted from higher TIC (3.09–3.16 dry wt%) in both cores. TOC (2.90–3.62 dry wt%) of the NHFC and NLFC did not differ considerable from ex situ data (2.91–3.40 dry wt%). Atomic C/N ratios were higher in both flow-through cores (8.67–9.43) compared to ex situ values (7.61–8.88), while TS was slightly lower (0.82–1.18 compared to 0.94–1.27 dry wt%), especially in the upper region (0–2 cm) of the NHFC (0.84 compared to 1.11 dry wt%) and showed, in contrast to the ex situ cores, no minimum at 4.5 cm sediment depth (Figs. 8c, 9c).

## 4 Discussion

### 4.1 The impact of fluid seepage and related processes on porewater gradients

Quepos Slide sediment cores that were studied ex situ showed a SMTZ and AOM peaks within the upper 20 cm of the sediment (Fig. 2). We are therefore confident that the SLOT experiments (core length 14–16 cm) contained the most active zone of the benthic methane filter. During the experiments, the depth of the SBTZ, as proxy for the SMTZ, was controlled by fluid flow and migrated over time. Fluid flow velocity in the low flow regime core (LFC,  $10.6 \text{ cm yr}^{-1}$ ) was in the same range of fluid flow modeled from the ex situ data ( $5\text{--}29 \text{ cm yr}^{-1}$ ). In the high flow regime core (HFC,  $106 \text{ cm yr}^{-1}$ ), the fluid flow was two to ten times higher compared to our modeled data and also higher than other values published for Quepos Slide ( $1\text{--}40 \text{ cm yr}^{-1}$ , Karaca et al., 2012); however, the flow was still in the range of neighboring seeps ( $0.1\text{--}200 \text{ cm yr}^{-1}$ , Hensen et al., 2004; Linke et al., 2005; Karaca et al., 2010; Krause et al., 2013). During the entire LFC experiment (before and after fluid flow change) no SBTZ developed. The missing evolution of a SBTZ was probably the result of a high hydrological residence time of the seepage medium (1080 days for the LFC and 108 days for the NHFC), i.e., the average time for the fluid to pass the entire sediment core. Nevertheless,

## Efficiency of the methane filter, Quepos Slide

P. Steeb et al.

Title Page

Abstract

Introduction

Conclusions

References

Tables

Figures



Back

Close

Full Screen / Esc

Printer-friendly Version

Interactive Discussion



## Efficiency of the methane filter, Quepos Slide

P. Steeb et al.

Title Page

Abstract

Introduction

Conclusions

References

Tables

Figures



Back

Close

Full Screen / Esc

Printer-friendly Version

Interactive Discussion



small amounts of the seepage fluid obviously passed through the entire sediment, probably facilitated through channeling (Torres et al., 2002; Wankel et al., 2012), as demonstrated by the presence of methane and bromide in the outflow. The fraction of seepage medium (calculated from  $\text{Br}^-$  concentration) emitted, relative to the total inflow seepage volume of the LFC, increased from 0 to 2.5 % in the last phase (260 days) and further increased to 4 % after the system was changed to high flow (NHFC). Low AOM activity was detected over the entire core after experiment termination with highest turnover between 7 and 9 cm sediment depth, while methane concentrations stayed continuously low around  $2\text{--}3\ \mu\text{molL}^{-1}$  over the entire core (see sampling artifacts, Sect. 3.2.3.). In the HFC experiment, the SBTZ and related AOM activity was much more pronounced than in the LFC. The SBTZ moved upwards from 14 cm (max. depth) to  $< 6$  cm, and dropped down to 10 cm sediment depth during the subsequent low flow phase (NLFC). During the first phase, fluids and SBTZ showed continuous migration, which was fast initially and became slower towards the end. The relatively stable depth of the SBTZ at the end of the first experiment phase (0–260 days) indicated the transition to a quasi-steady state situation. Highest AOM rates, determined by radiotracer measurements after experiment termination, were found within this SBTZ (6–10 cm sediment depth).

Sulfide concentrations of the HFC were generally highest within the SBTZ. In the LFC experiment, sulfide peaks were relatively broad and not so distinct, which was probably the result of a broad dispersive mixing layer between seepage and seawater medium. Due to the low fluid flow, higher sulfide concentrations evolved in the LFC as compared to the HFC, where sulfide was probably flushed-out before it accumulated. Relatively low sulfide concentrations were also observed at Mound 11, a seep site with high AOM and sulfate reduction activity and high fluid flow (Hensen et al., 2004; Krause et al., 2014). In the LFC experiments, sulfide concentrations fluctuated over time. While the increase in sulfide concentration was most likely correlated with enhanced sulfate reduction, a decrease could be caused either by the precipitation of metal sulfides and/or by microbial oxidation of sulfide (chemosynthesis).

## Efficiency of the methane filter, Quepos Slide

P. Steeb et al.

Title Page

Abstract

Introduction

Conclusions

References

Tables

Figures



Back

Close

Full Screen / Esc

Printer-friendly Version

Interactive Discussion



Precipitation of metal sulfides is correlated with a drop in pH (Glud et al., 2007; Preisler et al., 2007), as it was observed in our study. Oxygen and nitrate are important electron acceptors for microbial oxidation of sulfide in seep habitats. However, free oxygen was probably available only temporally (if at all) in the overlying water of the core due to a sampling artifact (see results), which was in accordance with a redox potential of less than 300 mV (Schulz, 2000). Moreover, sulfide oxidation with oxygen would create a drop in pH. Conversely, pH increased in the surface sediment, which could be caused by sulfide oxidation via dissimilatory nitrate reduction to ammonium. The process has been previously observed at the sediment–water interface of seeps system (de Beer et al., 2006). Nitrate availability in the seawater medium was limited ( $\sim 4 \mu\text{mol L}^{-1}$ ). Nevertheless, sulfide-oxidizing bacteria, such as *Beggiatoa* or *Thioploca* can accumulate nitrate in their vacuoles (Fossing et al., 1995; Preisler et al., 2007). Furthermore, sediment cores recovered from the field were covered by sulfide-oxidizing bacterial mats. Since oxygen concentration in the bottom water was extremely low in this OMZ ( $< 22 \mu\text{mol L}^{-1}$ , Wyrski, 1962; Levin, 2003), nitrate appears to be the most attractive electron acceptor for these sulfide oxidizers.

In summary, the observed increase in sulfide concentrations was most likely attributed to sulfate reduction activity, according to the development of the SBTZ. A loss of sulfide was caused by porewater flushing through advection, which was most pronounced in the HFC. Sulfide loss via oxidation with nitrate (top of the sediment) and sulfide precipitation (below 2 cm sediment depth) occurred more likely in the LFC.

### 4.2 Microbial turnover rates and efficiency of the benthic methane filter

Integrated areal AOM rates ( $45.15 \pm 11.48 \text{ mmol m}^{-2} \text{ d}^{-1}$ ) of the ex situ radiotracer measurements were in the upper range of previous modeled data ( $2.6\text{--}42.1 \text{ mmol m}^{-2} \text{ d}^{-1}$ ) and moderate to high compared to other seep systems (Treude et al., 2003; Joye et al., 2004; Niemann et al., 2006; Knittel and Boetius, 2009; Krause et al., 2014). In the SLOT experiments, the calculated methane flux ( $0.3\text{--}2.8 \text{ mmol m}^{-2} \text{ d}^{-1}$ ) was lower compared to modeled flux ( $9.1\text{--}45.1 \text{ mmol m}^{-2} \text{ d}^{-1}$ ) of the replicate core and at the

## Efficiency of the methane filter, Quepos Slide

P. Steeb et al.

Title Page

Abstract

Introduction

Conclusions

References

Tables

Figures



Back

Close

Full Screen / Esc

Printer-friendly Version

Interactive Discussion



lower limit of the previously modeled data ( $1.5\text{--}58.0\text{ mmol m}^{-2}\text{ d}^{-1}$ , Karaca et al., 2012). However, fluxes of the SLOT experiment were still in the range of data published for seeps in this region (Mau et al., 2006; Karaca et al., 2010). In agreement with the relatively low methane flux during the SLOT experiment, AOM rates (determined from the difference in methane concentration between in and outflow) were 1 to 2 orders of magnitude lower compared to ex situ determinations. AOM rates determined with radiotracer measurements after experiment termination revealed peaks within the SBTZ (proxy for the SMTZ) of the HFC (4–10 cm b.s.f.). A broader distribution of AOM was found in the LFC, while similar integrated rates suggest the same potential for AOM. This agreement of integrated AOM rates despite differences in fluid flux illustrates a widening of the AOM zone with lower fluid fluxes, while a narrow AOM zone at high fluxes appears to be compensated by higher methane turnover. This effect was also reflected in a more distinct peak of sulfide (see above) and confirmed by simulations in the numerical model, specifically at the two model runs from SO206-31 (MUC) (Figs. 1 and 2). However, it should be kept in mind that methane concentrations during the experiment were much lower than expected than under in situ pressure and it is therefore difficult to predict the upper limit of the balance between fluid flux and AOM activity.

While in a previous study the methane consumption efficiency of the benthic filter was estimated to range between 23 and 96 % of the methane flux (Karaca et al., 2012), the efficiency in our study was between 92 and 100 % in the modeled ex situ data and 99 % for the experimental setup (under the assumption of steady-state conditions directly before fluid flow change). A reason for the partial disagreement in efficiency compared to the earlier studies could be the natural variability of methane fluxes in this highly heterogeneous area. While Karaca et al. (2012) based their results on a large number of sediment cores (20 cores from the same seep site), only two randomly chosen sites were sampled in our study, and only one was used for the experiment. Another explanation could be temporal variability of fluid and methane flux. Karaca et al. (2012) conducted their study 10 years prior to ours. Methane flux as well as

## Efficiency of the methane filter, Quepos Slide

P. Steeb et al.

Title Page

Abstract

Introduction

Conclusions

References

Tables

Figures



Back

Close

Full Screen / Esc

Printer-friendly Version

Interactive Discussion



microbial activity could have changed easily over this period (Mau et al., 2007; Füre et al., 2010). A drop in methane flux would probably enhance the efficiency of the benthic methane filter. For example, in the present experiment, methane fluxes were 2 to 33 times lower compared to the model of Karaca et al. (2012) since the system was not pressurized and hence the solubility of methane was limited. Lower methane fluxes resulted in a high efficiency of the benthic microbial methane filter, despite relatively high fluid advection.

Radiotracer determination of microbial turnover rates after the experiment revealed sulfate reduction activity at levels higher than AOM, which was probably partly coupled to organic matter degradation. Since the cores were obtained within an oxygen minimum zone, sulfate reduction is supposedly the most important pathway for organic matter degradation (Jørgensen 1977; Sørensen et al., 1979; Bohlen et al., 2011). High C/N ratios in cores of the terminated experiment compared to ex situ cores (Figs. 8 and 9) support this assumption, because advanced microbial degradation of fresh organic matter with high nitrogen content leads to a shift from low to high C/N ratios (Whiticar, 2002). We assume that around 80 % of the sulfate reduction in the ex situ analyses of SO206-St31 (MUC) was probably related to organic matter degradation (AOM: SR = 0.21). Admittedly, this ratio was likely overestimated, because ex situ radiotracer incubations were conducted under atmospheric pressure and less methane was available compared to the in situ conditions. However, because organoclastic sulfate reduction occurred ex situ at the sediment–water interface (0–2 cm b.s.f., Figs. 1 and 2), where the consumed sulfate is replenished relatively rapidly by diffusion and mixing from the seawater, its activity has probably only little effect on sulfate gradients deeper in the sediment (Jørgensen et al., 2001; Karaca et al., 2012).

In Summary, the benthic microbial methane filter at Quepos Slide was found to be very efficient under continuous flow. Only increases in fluid and methane flux, such as at the beginning of the experiment or more pronounced after the fluid flow change, led to a drop in efficiency. Once a new steady state situation establishes, higher fluxes are expected to be compensated by a more intensive AOM zone (see above).

### 4.3 Response time of the microbial benthic methane filter

In the outflow of the LFC, methane concentrations increased only little and decreased after 202 days (directly before fluid flow change) to the initial concentration. In contrast, methane concentrations in the outflow of the HFC core were high ( $7.5 \mu\text{mol L}^{-1}$ ) at the beginning (29 days) and decreased quasi-exponentially to concentrations of  $\sim 2 \mu\text{mol L}^{-1}$  after 171 days. In the same time interval, the fraction of the methane-containing “seepage” medium at the sediment–water interface, calculated from the tracer (bromide) concentrations, changed from 13 to 34 %, (Fig. 4a, j). From the delivered methane ( $125.5$  and  $376.4 \mu\text{mol L}^{-1}$ ) 30 and 98 %, was oxidized after 29 and 171 days, respectively, in the HFC. This period (0–171 days) can be interpreted as the response time of the benthic microbial methane filter in the sediments of Quepos Slide. After change of the flow regime, the efflux of methane suddenly reduced to only 22 % ( $0.009 \text{ mmol m}^{-2} \text{ d}^{-1}$ ) in the former HFC (= NLFC), while the efflux in the former LFC (= NHFC) increased rapidly 15-fold ( $0.169 \text{ mmol m}^{-2} \text{ d}^{-1}$ ) after changing the fluid flow. Based on bromide concentrations, the fraction of seepage medium in the outflow of the NHFC was 4 %, which should theoretically equal  $38.5 \mu\text{mol L}^{-1}$  methane in the outflow, if no methane would be consumed. Compared to methane concentrations directly measured in the outflow, only  $\sim 70$  % of the inflow methane was oxidized and 30 % was emitted.

These results illustrate how sudden events could result in an abrupt increase in methane efflux. Mau et al. (2006) attributed fluctuations of methane concentrations in the water column, which occurred between autumn 2002 and 2003 at the Costa Rican seeps, to an earthquake in June 2002. However, it was not specified if the increased methane flux resulted from increased fluid flow, or simply from bubble release or if it was a continuous increase of methane flux or just a transient effect.

The experiments of the present study clearly show that the benthic microbial methane filter is able to respond within a relatively brief time of 5–6 months to increased methane fluxes and leads to the development of a much shallower and thinner AOM

## Efficiency of the methane filter, Quepos Slide

P. Steeb et al.

Title Page

Abstract

Introduction

Conclusions

References

Tables

Figures



Back

Close

Full Screen / Esc

Printer-friendly Version

Interactive Discussion



## Efficiency of the methane filter, Quepos Slide

P. Steeb et al.

Title Page

Abstract

Introduction

Conclusions

References

Tables

Figures



Back

Close

Full Screen / Esc

Printer-friendly Version

Interactive Discussion



zone. Even if methane fluxes and methane concentrations were four times higher in situ, as expected from modeled methane fluxes of this study, the benthic microbial methane filter may still be able to respond quickly if a methanotrophic community is already fully established. Outside of seep habitats, where the microbial benthic methane filter is either absent or in deeper sediment zones, the adaptation might require much more time, since the doubling rate of the microbes involved is in the order of a few months (Girguis et al., 2005; Nauhaus et al., 2007; Krüger et al., 2008; Meulepas et al., 2009). Mau et al. (2007) observed a reduction of methane emissions in the water column above the earthquake-impacted seepage area by 50–90 % in a period of one year. In our experiments, the benthic microbial methane filter required only ~ 170 days to adapt to the new flow regime. It is not clear, if the subsequent reduction of methane emissions observed by Mau et al. (2007) was the result of an ephemeral pulse of methane flux or by the adaptation of the microbial benthic methane filter. Our results indicate that at least both situations are conceivable.

Another scenario, in which the benthic methane filter would be challenged, is the destabilization of gas hydrates as a result of climate change (Buffett and Archer, 2004). However, due to retarded heat flux into deeper sediment layers, dissociation of considerable gas hydrate volumes probably require hundreds to thousands of years (Biastoch et al., 2011). In the present study, we demonstrate that an established microbial benthic methane filter can compensate slow, abrupt increases in methane flux. Only “pristine” sediments, which are virtually devoid of methanotrophs are expected to show long adaptations periods of up to several years or even decades (Dale et al., 2008) due to slow growth rates of the anaerobes (Girguis et al., 2005; Nauhaus et al., 2007; Goffredi et al., 2008).

## 5 Conclusions

Surface sediments of the Quepos Slide, a cold seep on the Pacific coastline of Costa Rica located within the Eastern Tropical North Pacific oxygen minimum zone,

## Efficiency of the methane filter, Quepos Slide

P. Steeb et al.

[Title Page](#)

[Abstract](#)

[Introduction](#)

[Conclusions](#)

[References](#)

[Tables](#)

[Figures](#)



[Back](#)

[Close](#)

[Full Screen / Esc](#)

[Printer-friendly Version](#)

[Interactive Discussion](#)



feature a highly efficient benthic methane filter, which was confirmed by (1) direct measurements of methane turnover rates *ex situ*, (2) a numerical reaction model, and (3) *in vitro* experiments with intact sediment cores using a sediment-flow-through system. The flow-through system further allowed following the adaptation of the SMTZ to changes in fluid flow showing that the SMTZ narrows to a thin layer under high fluid flow conditions. Methane transported under high fluid flow (but at atmospheric pressure) was efficiently consumed (99 % oxidation) by the benthic methane filter after a response period of 150–170 days. These results illustrate how an established benthic methanotrophic microbial community could react to pulses in fluid and methane flow induced, for example, by earthquakes or gas hydrate dissociation, and how it regains its efficiency level after passing through a non-steady state period.

*Author contributions.* T. Treude, P. Linke, and C. Hensen initiated this study. P. Steeb, S. Krause, M. Nuzzo, A. Dale, sampled the sediment. S. Krause and P. Steeb performed the radiotracer incubations. On board, A. Dale was responsible for porewater measurements and M. Nuzzo conducted the methane measurements. C. Hensen and P. Steeb carried out the numerical modeling with input from A. Dale. S. Krause and P. Steeb carried out rate measurements and turnover calculations. Experiments were designed by T. Treude and P. Linke. Experiments were performed by P. Steeb including measurements and calculations. P. Steeb wrote the manuscript with input T. Treude, P. Linke, and A. Dale as well as other co-authors.

*Acknowledgements.* We thank the captain and the crew of R/V *SONNE* and all staff members who this supported work onboard. Special thanks goes to B. Domeyer, A. Bleyer, R. Ebbinghaus, R. Surberg, E. Corrales-Cordero, and E. Pinero for technical support during porewater analyzes. K. Kretschmer is thanked for help during maintenance of the SLOT-system. K. Kretschmer, J. Farkas, and J. Hommer are thanked for technical support during radiotracer analyzes. This project was financed through the Collaborative Research Center (SFB) 574 “Volatiles and Fluids in Subduction Zones” and the Cluster of Excellence “The Future Ocean” funded by the German Research Foundation (DFG). M. Nuzzo was funded by the Portuguese Science and Technology Foundation post-doctoral fellowship FCT-SFRH/BPD/44598/2008.

The service charges for this open access publication have been covered by a Research Centre of the Helmholtz Association.

## References

- 5 Aiello, I. W.: Fossil seep structures of the Monterey Bay region and tectonic/structural controls on fluid flow in an active transform margin, *Palaeogeogr. Palaeoclimatol.*, 227, 124–142, 2005.
- De Beer, D., Sauter, E., Niemann, H., Kaul, N., Witte, U., Schlüter, M., and Boetius, A.: In situ fluxes and zonation of microbial activity in surface sediments of the Håkon Mosby Mud Volcano, *Limnol. Oceanogr.*, 51, 1315–1331, 2006.
- 10 Biastoch, A., Treude, T., Rüpke, L. H., Riebesell, U., Roth, C., Burwicz, E. B., Park, W., Latif, M., Böning, C. W., Madec, G., and Wallmann, K.: Rising Arctic Ocean temperatures cause gas hydrate destabilization and ocean acidification, *Geophys. Res. Lett.*, 38, 1–5, 2011.
- Boetius, A., Ravensschlag, K., Schubert, C. J., Rickert, D., Widdel, F., Gieseke, A., Amann, R., Jørgensen, B. B., Witte, U., Pfannkuche, O., and Jørgensen, B. B.: A marine microbial consortium apparently mediating anaerobic oxidation of methane, *Nature*, 407, 623–626, 2000.
- 15 Bohlen, L., Dale, A. W., Sommer, S., Mosch, T., Hensen, C., Noffke, A., Scholz, F., and Wallmann, K.: Benthic nitrogen cycling traversing the Peruvian oxygen minimum zone, *Geochim. Cosmochim. Ac.*, 75, 6094–6111, 2011.
- 20 Bohrmann, G., Heeschen, K., Jung, C., Weinrebe, W., Baranov, B., Heath, R., Hu, V., Hort, M., and Masson, D.: Widespread fluid expulsion along the seafloor of the Costa Rica convergent margin, *Terra Nov.*, 14, 69–79, 2002.
- Borowski, W. S., Paull, C. K., and Ussler III., W.: Marine pore-water sulfate profiles indicate in situ methane flux from underlying gas hydrate, *Geology*, 24, 655–658, 1996.
- 25 Borowski, W. S., Paull, C. K., and Ussler III., W.: Global and local variations of interstitial sulfate gradients in deep-water, continental margin sediments: sensitivity to underlying methane and gas hydrates, *Mar. Geol.*, 159, 131–154, 1999.
- Buffett, B. and Archer, D.: Global inventory of methane clathrate: sensitivity to changes in the deep ocean, *Earth Planet. Sc. Lett.*, 227, 185–199, 2004.

## Efficiency of the methane filter, Quepos Slide

P. Steeb et al.

Title Page

Abstract

Introduction

Conclusions

References

Tables

Figures



Back

Close

Full Screen / Esc

Printer-friendly Version

Interactive Discussion



**Efficiency of the  
methane filter,  
Quepos Slide**

P. Steeb et al.

[Title Page](#)[Abstract](#)[Introduction](#)[Conclusions](#)[References](#)[Tables](#)[Figures](#)[Back](#)[Close](#)[Full Screen / Esc](#)[Printer-friendly Version](#)[Interactive Discussion](#)

Burwicz, E., Rüpke, L., and Wallmann, K.: Estimation of the global amount of submarine gas hydrates formed via microbial methane formation based on numerical reaction-transport modeling and a novel parameterization of Holocene sedimentation, *Geochim. Cosmochim. Ac.*, 75, 4562–4576, 2011.

5 Cline, J.: Spectrophotometric determination of hydrogen sulfide in natural waters, *Limnol. Oceanogr.*, 14, 454–458, 1969.

Crutchley, G. J., Klaeschen, D., Planert, L., Bialas, J., Berndt, C., Papenberg, C., Hensen, C., Hornbach, M. J., Krastel, S., and Brueckmann, W.: The impact of fluid advection on gas hydrate stability: investigations at sites of methane seepage offshore Costa Rica, *Earth Planet. Sc. Lett.*, 401, 95–109, 2014.

10 Dale, A. W., Brüchert, V., Alperin, M., and Regnier, P.: An integrated sulfur isotope model for Namibian shelf sediments, *Geochim. Cosmochim. Ac.*, 73, 1924–1944, 2009.

Dale, A. W., Van Cappellen, P., Aguilera, D. R., and Regnier, P.: Methane efflux from marine sediments in passive and active margins: estimations from bioenergetic reaction–transport simulations, *Earth Planet. Sc. Lett.*, 265, 329–344, 2008.

15 Dalsgaard, T., Nielsen, L. P., Brotas, V., Viaroli, P., Underwood, G., Nedwell, D., Sundbäck, K., Rysgaard, S., Miles, A., Bartoli, M., Dong, L., Thornton, D. C. O., Ottosen, L. D. M., Castaldelli, G., and Risgaard-Petersen, N.: Sediment characteristics, in: *Protocol Handbook for NICE – Nitrogen Cycling in Estuaries: a Project Under EU Research Programme: Marine Science and Technology (MAST III)*, National Environmental Research Institute, Silkeborg, Denmark, 53–54, 2000.

20 Ettwig, K. F., Butler, M. K., Le Paslier, D., Pelletier, E., Mangenot, S., Kuypers, M. M. M., Schreiber, F., Dutilh, B. E., Zedelius, J., de Beer, D., Gloerich, J., Wessels, H. J. C. T., van Alen, T., Luesken, F., Wu, M. L., van de Pas-Schoonen, K. T., Op den Camp, H. J. M., Janssen-Megens, E. M., Francoijs, K.-J., Stunnenberg, H., Weissenbach, J., Jetten, M. S. M., and Strous, M.: Nitrite-driven anaerobic methane oxidation by oxygenic bacteria, *Nature*, 464, 543–8, 2010.

Fischer, D., Mogollón, J. M., Strasser, M., Pape, T., Bohrmann, G., Fekete, N., Spiess, V., and Kasten, S.: Subduction zone earthquake as potential trigger of submarine hydrocarbon seepage, *Nat. Geosci.*, 6, 647–651, 2013.

30 Fischer, D., Sahling, H., and Nöthen, K.: Interaction between hydrocarbon seepage, chemosynthetic communities, and bottom water redox at cold seeps of the Makran

## Efficiency of the methane filter, Quepos Slide

P. Steeb et al.

Title Page

Abstract

Introduction

Conclusions

References

Tables

Figures



Back

Close

Full Screen / Esc

Printer-friendly Version

Interactive Discussion



accretionary prism: insights from habitat-specific pore water sampling and modeling, *Biogeochemistry*, 9, 2013–2031, 2012.

Fossing, H., Gallardo, V., Jørgensen, B., Hüttel, M., Nielson, L. P., Schulz, H., Canfield, D. E., Forster, S., Glud, R. N., Gundersen, J. K., Küver, J., Ramsing, N. B., Teske, A., Thamdrup, B., and Ulloa, O.: Concentration and transport of nitrate by the mat-forming sulphur bacterium *Thioploca*, *Nature*, 374, 714–715, 1995.

Füri, E., Hilton, D. R., Tryon, M. D., Brown, K. M., McMurtry, G. M., Brückmann, W., and Wheat, C. G.: Carbon release from submarine seeps at the Costa Rica fore arc: implications for the volatile cycle at the Central America convergent margin, *Geochem. Geophys. Geos.*, 11, Q04S21, doi:10.1029/2009GC002810, 2010.

Girguis, P., Cozen, A., and DeLong, E.: Growth and population dynamics of anaerobic methane-oxidizing archaea and sulfate-reducing bacteria in a continuous-flow bioreactor, *Appl. Environ. Microbiol.*, 71, 3725–3733, 2005.

Glud, R. N., Berg, P., Fossing, H., and Jørgensen, B. B.: Effect of the diffusive boundary layer on benthic mineralization and  $O_2$  distribution: a theoretical model analysis, *Limnol. Oceanogr.*, 52, 547–557, 2007.

Goffredi, S. K., Wilpiseski, R., Lee, R., and Orphan, V. J.: Temporal evolution of methane cycling and phylogenetic diversity of archaea in sediments from a deep-sea whale-fall in Monterey Canyon, California, *ISME J.*, 2, 204–20, 2008.

Han, X., Suess, E., Sahling, H., and Wallmann, K.: Fluid venting activity on the Costa Rica margin: new results from authigenic carbonates, *Int. J. Earth Sci.*, 93, 596–611, 2004.

Harders, R., Ranero, C. R., Weinrebe, W., and Behrmann, J. H.: Submarine slope failures along the convergent continental margin of the Middle America Trench, *Geochem. Geophys. Geos.*, 12, Q05S32, doi:10.1029/2010GC003401, 2011.

Henrys, S., Reyners, M., Pecher, I., Bannister, S., Nishimura, Y., and Maslen, G.: Kinking of the subducting slab by escalator normal faulting beneath the North Island of New Zealand, *Geology*, 34, 777–780, 2006.

Hensen, C. and Wallmann, K.: Methane formation at Costa Rica continental margin – constraints for gas hydrate inventories and cross-décollement fluid flow, *Earth Planet. Sc. Lett.*, 236, 41–60, 2005.

Hensen, C., Wallmann, K., Schmidt, M., Ranero, C. R., and Suess, E.: Fluid expulsion related to mud extrusion off Costa Rica – A window to the subducting slab, *Geology*, 32, 201–204, doi:10.1130/G20119.1, 2004.

## Efficiency of the methane filter, Quepos Slide

P. Steeb et al.

Title Page

Abstract

Introduction

Conclusions

References

Tables

Figures



Back

Close

Full Screen / Esc

Printer-friendly Version

Interactive Discussion



- Hesse, R., Frappe, S. K., Egeberg, P. K., and Matsumoto, R.: Stable Isotope Studies (Cl, O, and H) of Interstitial Waters from Site 997, Blake Ridge Gas Hydrate Field, West Atlantic, Proceedings of the Ocean Drilling Program – Scientific Results, 164, 129–137, 2000.
- Hinrichs, K. and Boetius, A.: The anaerobic oxidation of methane: new insights in microbial ecology and biogeochemistry, in: Ocean Margin Systems, edited by: Wefer, G., Billet, D., Hebbeln, D., Jørgensen, B., Schlüter, M., and Van Weering, T., Springer-Verlag, Berlin Heidelberg, 457–477, 2002.
- Ivanenkov, V. N. and Lyakhin, Y. I.: Determination of total alkalinity in seawater, in: Methods of Hydrochemical Investigations in the Ocean, edited by: Bordovsky, O. K. and Ivanenkov, V. N., Nauka Publ. House, Moscow, 110–114, 1978.
- Jørgensen, B. B.: The sulfur cycle of a coastal marine sediment (Limfjorden, Denmark), *Limnol. Oceanogr.*, 22, 814–832, 1977.
- Jørgensen, B. B.: A comparison of methods for the quantification of bacterial sulfate reduction in coastal marine sediments. 1. Measurements with radiotracer techniques, *Geomicrobiol. J.*, 1, 11–27, 1978.
- Jørgensen, B., Weber, A., and Zopfi, J.: Sulfate reduction and anaerobic methane oxidation in Black Sea sediments, *Deep-Sea Res. Pt. I*, 48, 2097–2120, 2001.
- Joye, S. B., Boetius, A., Orcutt, B. N., Montoya, J. P., Schulz, H. N., Erickson, M. J., and Lugo, S. K.: The anaerobic oxidation of methane and sulfate reduction in sediments from Gulf of Mexico cold seeps, *Chem. Geol.*, 205, 219–238, 2004.
- Judd, A., Hovland, M., and Dimitrov, L.: The geological methane budget at continental margins and its influence on climate change, *Geofluids*, 2, 109–126, 2002.
- Kallmeyer, J., Ferdelman, T. G., Weber, A., Fossing, H., and Jørgensen, B. B.: A cold chromium distillation procedure for radiolabeled sulfide applied to sulfate reduction measurements, *Limnol. Oceanogr.-Meth.*, 2, 171–180, 2004.
- Karaca, D., Hensen, C., and Wallmann, K.: Controls on authigenic carbonate precipitation at cold seeps along the convergent margin off Costa Rica, *Geochem. Geophys. Geosy.*, 11, 1–19, 2010.
- Karaca, D., Schleicher, T., Hensen, C., Linke, P., and Wallmann, K.: Quantification of methane emission from bacterial mat sites at Quepos Slide offshore Costa Rica, *Int. J. Earth Sci.*, 103, 1–25, 2012.
- Kluesner, J. W., Silver, E. A., Bangs, N. L., McIntosh, K. D., Gibson, J., Orange, D., Ranero, C. R., and von Huene, R.: High density of structurally controlled, shallow to deep

## Efficiency of the methane filter, Quepos Slide

P. Steeb et al.

Title Page

Abstract

Introduction

Conclusions

References

Tables

Figures



Back

Close

Full Screen / Esc

Printer-friendly Version

Interactive Discussion



water fluid seep indicators imaged offshore Costa Rica, *Geochem. Geophys. Geosy.*, 14, 519–539, 2013.

Knittel, K. and Boetius, A.: Anaerobic oxidation of methane: progress with an unknown process, *Annu. Rev. Microbiol.*, 63, 311–34, 2009.

5 Krause, S., Steeb, P., Hensen, C., Liebetrau, V., Dale, A. W., Nuzzo, M., and Treude, T.: Microbial activity and carbonate isotope signatures as a tool for identification of spatial differences in methane advection: a case study at the Pacific Costa Rican margin, *Biogeosciences*, 11, 507–523, doi:10.5194/bg-11-507-2014, 2014.

10 Krüger, M., Blumenberg, M., Kasten, S., Wieland, A., Känel, L., Klock, J., Michaelis, W., and Seifert, R.: A novel, multi-layered methanotrophic microbial mat system growing on the sediment of the Black Sea, *Environ. Microbiol.*, 10, 1934–47, 2008.

Kutterolf, S., Liebetrau, V., Mörz, T., Freundt, A., Hammerich, T., and Garbe-Schönberg, D.: Lifetime and cyclicity of fluid venting at forearc mound structures determined by tephrostratigraphy and radiometric dating of authigenic carbonates, *Geology*, 36, 707–710, 2008.

15 Kvenvolden, K.: Methane hydrate in the global organic carbon cycle, *Terra Nov.*, 14, 302–306, 2002.

Levin, L. A.: Oxygen minimum zone benthos: adaption and community, *Oceanogr. Mar. Biol.*, 41, 1–45, 2003.

20 Linke, P., Wallmann, K., Suess, E., Hensen, C., and Rehder, G.: In situ benthic fluxes from an intermittently active mud volcano at the Costa Rica convergent margin, *Earth Planet. Sc. Lett.*, 235, 79–95, 2005.

Mau, S., Sahling, H., Rehder, G., Suess, E., Linke, P., and Soeding, E.: Estimates of methane output from mud extrusions at the erosive convergent margin off Costa Rica, *Mar. Geol.*, 225, 129–144, 2006.

25 Mau, S., Rehder, G., Arroyo, I. G., Gossler, J., and Suess, E.: Indications of a link between seismotectonics and CH<sub>4</sub> release from seeps off Costa Rica, *Geochem. Geophys. Geosy.*, 8, 1–13, 2007.

30 Mau, S., Rehder, G., Sahling, H., Schleicher, T., and Linke, P.: Seepage of methane at Jaco Scar, a slide caused by seamount subduction offshore Costa Rica, *Int. J. Earth Sci.*, doi:10.1007/s00531-012-0822-z, 2012.

**Efficiency of the  
methane filter,  
Quepos Slide**

P. Steeb et al.

[Title Page](#)[Abstract](#)[Introduction](#)[Conclusions](#)[References](#)[Tables](#)[Figures](#)[Back](#)[Close](#)[Full Screen / Esc](#)[Printer-friendly Version](#)[Interactive Discussion](#)

- Meulepas, R. J. W., Jagersma, C. G., Gieteling, J., Buisman, C. J. N., Stams, A. J. M., and Lens, P. N. L.: Enrichment of anaerobic methanotrophs in sulfate-reducing membrane bioreactors, *Biotechnol. Bioeng.*, 104, 458–70, 2009.
- Milucka, J., Ferdelman, T. G., Polerecky, L., Franzke, D., Wegener, G., Schmid, M., Lieberwirth, I., Wagner, M., Widdel, F., and Kuypers, M. M. M.: Zero-valent sulphur is a key intermediate in marine methane oxidation, *Nature*, 2, 1–23, 2012.
- Minami, H., Tatsumi, K., Hachikubo, A., Yamashita, S., Sakagami, H., Takahashi, N., Shoji, H., Jin, Y. K., Obzhirov, A., Nikolaeva, N., and Derkachev, A.: Possible variation in methane flux caused by gas hydrate formation on the northeastern continental slope off Sakhalin Island, Russia, *Geo-Mar. Lett.*, 32, 525–534, 2012.
- Nauhaus, K., Albrecht, M., Elvert, M., Boetius, A., and Widdel, F.: In vitro cell growth of marine archaeal-bacterial consortia during anaerobic oxidation of methane with sulfate, *Environ. Microbiol.*, 9, 187–96, 2007.
- Niemann, H., Lösekann, T., de Beer, D., Elvert, M., Nadalig, T., Knittel, K., Amann, R., Sauter, E. J., Schlüter, M., Klages, M., Foucher, J. P., and Boetius, A.: Novel microbial communities of the Haakon Mosby mud volcano and their role as a methane sink, *Nature*, 443, 854–8, 2006.
- Orcutt, B. N., Sylvan, J. B., Knab, N. J., and Edwards, K. J.: Microbial ecology of the dark ocean above, at, and below the seafloor, *Microbiol. Mol. Biol. R.*, 75, 361–422, 2011.
- Preisler, A., de Beer, D., Lichtschlag, A., Lavik, G., Boetius, A., and Jørgensen, B. B.: Biological and chemical sulfide oxidation in a Beggiatoa inhabited marine sediment, *ISME J.*, 1, 341–53, 2007.
- Ranero, C. and von Huene, R.: Subduction erosion along the Middle America convergent margin, *Nature*, 404, 748–52, 2000.
- Ranero, C. R., Grevemeyer, I., Sahling, H., Barckhausen, U., Hensen, C., Wallmann, K., Weinrebe, W., Vannucchi, P., von Huene, R., and McIntosh, K.: Hydrogeological system of erosional convergent margins and its influence on tectonics and interplate seismogenesis, *Geochem. Geophys. Geosy.*, 9, 707–710, doi:10.1029/2007GC001679, 2008.
- Reeburgh, W. S.: Oceanic methane biogeochemistry, *Chem. Rev.*, 107, 486–513, 2007.
- Sahling, H., Masson, D. G., Ranero, C. R., Hühnerbach, V., Weinrebe, W., Klauke, I., Bürk, D., Brückmann, W., and Suess, E.: Fluid seepage at the continental margin offshore Costa Rica and southern Nicaragua, *Geochem. Geophys. Geosy.*, 9, 1–22, 2008.

**Efficiency of the  
methane filter,  
Quepos Slide**

P. Steeb et al.

[Title Page](#)[Abstract](#)[Introduction](#)[Conclusions](#)[References](#)[Tables](#)[Figures](#)[Back](#)[Close](#)[Full Screen / Esc](#)[Printer-friendly Version](#)[Interactive Discussion](#)

Sahling, H., Rickert, D., Lee, R. W., Linke, P., and Suess, E.: Macrofaunal community structure and sulfide flux at gas hydrate deposits from the Cascadia convergent margin, NE Pacific, *Mar. Ecol.-Prog. Ser.*, 231, 121–138, 2002.

Schmidt, M., Hensen, C., Mörz, T., Müller, C., Grevemeyer, I., Wallmann, K., Mau, S., and Kaul, N.: Methane hydrate accumulation in “Mound 11” mud volcano, Costa Rica forearc, *Mar. Geol.*, 216, 83–100, 2005.

Schulz, H. D.: Redox measurements in marine sediments, in: *REDOX: Fundamentals, Processes, and Applications*, edited by: Schüring, J., Schulz, H. D., Böttcher, J., and Duijnvisveld, W. H. M., Springer, Berlin, 235–246, 2000.

Sørensen, J., Jørgensen, B., and Revsbech, N.: A comparison of oxygen, nitrate, and sulfate respiration in coastal marine sediments, *Microb. Ecol.*, 5, 105–115, 1979.

Steeb, P., Linke, P., and Treude, T.: A sediment flow-through system to study the impact of shifting fluid and methane flow regimes on the efficiency of the benthic methane filter, *Limnol. Oceanogr.-Meth.*, 12, 25–45, 2014.

Suess, E.: Marine cold seeps, in: *Handbook of Hydrocarbon and Lipid Microbiology*, edited by: Timmis, K. N., Springer, Berlin Heidelberg, 188–198, 2010.

Syracuse, E. M. and Abers, G. A.: Global compilation of variations in slab depth beneath arc volcanoes and implications, *Geochem. Geophys. Geosy.*, 7, 1–18, 2006.

Tishchenko, P., Hensen, C., Wallmann, K., and Wong, C. S.: Calculation of the stability and solubility of methane hydrate in seawater, *Chem. Geol.*, 219, 37–52, 2005.

Torres, M. E. E., Wallmann, K., Tréhu, A. M. M., Bohrmann, G., Borowski, W. S., and Tomaru, H.: Gas hydrate growth, methane transport, and chloride enrichment at the southern summit of Hydrate Ridge, Cascadia margin off Oregon, *Earth Planet. Sc. Lett.*, 226, 168–175, 2004.

Torres, M. E., McManus, J., Hammond, D. E., de Angelis, M. A., Heeschen, K. U., Colbert, S. L., Tryon, M. D., Brown, K. M., and Suess, E.: Fluid and chemical fluxes in and out of sediments hosting methane hydrate deposits on Hydrate Ridge, OR, I: Hydrological provinces, *Earth Planet. Sc. Lett.*, 201, 525–540, 2002.

Treude, T., Boetius, A., Knittel, K., Wallmann, K., and Barker Jørgensen, B.: Anaerobic oxidation of methane above gas hydrates at Hydrate Ridge, NE Pacific Ocean, *Mar. Ecol.-Prog. Ser.*, 264, 1–14, 2003.

Treude, T., Krüger, M., Boetius, A., and Jørgensen, B.: Environmental control on anaerobic oxidation of methane in the gassy sediments of Eckernförde Bay (German Baltic), *Limnol. Oceanogr.*, 50, 1771–1786, 2005.

## Efficiency of the methane filter, Quepos Slide

P. Steeb et al.

Title Page

Abstract

Introduction

Conclusions

References

Tables

Figures



Back

Close

Full Screen / Esc

Printer-friendly Version

Interactive Discussion



Tryon, M. D., Brown, K. M., and Torres, M. E.: Fluid and chemical fluxes in and out of sediments hosting methane hydrate deposits on Hydrate Ridge, OR, II: Hydrological provinces, Earth Planet. Sc. Lett., 201, 541–557, 2002.

Tryon, M. D., Wheat, C. G., and Hilton, D. R.: Fluid sources and pathways of the Costa Rica erosional convergent margin, Geochem. Geophys. Geosy., 11, Q04S22, doi:10.1029/2009GC002818, 2010.

Visser, W., Scheffers, W. A., Batenburg-van der Vegte, W. H., and van Dijken, J. P.: Oxygen requirements of yeasts, Appl. Environ. Microb., 56, 3785–3792, 1990.

Wallmann, K., Pinero, E., Burwicz, E., Haeckel, M., Hensen, C., Dale, A., and Ruepke, L.: The global inventory of methane hydrate in marine sediments: a theoretical approach, Energies, 5, 2449–2498, 2012.

Wankel, S. D., Adams, M. M., Johnston, D. T., Hansel, C. M., Joye, S. B., and Girguis, P. R.: Anaerobic methane oxidation in metalliferous hydrothermal sediments: influence on carbon flux and decoupling from sulfate reduction, Environ. Microbiol., 14, 2726–40, 2012.

Whiticar, M. J.: Diagenetic relationships of methanogenesis, nutrients, acoustic turbidity, pockmarks and freshwater seepages in Eckernförde Bay, Mar. Geol., 182, 29–53, 2002.

Widdel, F. and Bak, F.: Gram-negative mesophilic sulfate-reducing bacteria, in: The Prokaryotes, edited by: Dworkin, M., Falkow, S., Rosenberg, E., Schleifer, K.-H., and Stackebrandt, E., Springer US, New York, 3352–3378, 2006.

Wyrтки, K.: The oxygen minima in relation to ocean circulation, Deep-Sea Res., 9, 11–23, 1962.

## BGD

11, 16033–16083, 2014

## Efficiency of the methane filter, Quepos Slide

P. Steeb et al.

[Title Page](#)
[Abstract](#)
[Introduction](#)
[Conclusions](#)
[References](#)
[Tables](#)
[Figures](#)

[Back](#)
[Close](#)
[Full Screen / Esc](#)
[Printer-friendly Version](#)
[Interactive Discussion](#)


**Table 1.** Sampling sites of the Quepos Slide and the SMTZ depth in cm below seafloor (b.s.f.).

Station	Latitude (N)	Longitude (W)	Water depth m	Depth of SMTZ cm b.s.f.
SO206-29 (MUC)	8°51.29′	84°12.60′	402	12.5–22.5
SO206-31 (MUC)	8°51.12′	84°13.06′	399	5.0–15.0

## Efficiency of the methane filter, Quepos Slide

P. Steeb et al.

[Title Page](#)

[Abstract](#)

[Introduction](#)

[Conclusions](#)

[References](#)

[Tables](#)

[Figures](#)

[◀](#)

[▶](#)

[◀](#)

[▶](#)

[Back](#)

[Close](#)

[Full Screen / Esc](#)

[Printer-friendly Version](#)

[Interactive Discussion](#)



**Table 2.** Salt concentrations of the two different media used in the SLOT-system. Seawater medium with sulfate was delivered from the top, seepage medium with methane and without sulfate from the bottom. In the last line, the gas in the respective medium headspace is denoted.

Salts (all in mmol l <sup>-1</sup> )	Seawater medium (with SO <sub>4</sub> <sup>2-</sup> )	Seepage medium (with CH <sub>4</sub> )*
KBr	0.006	0.756
KCl	8.05	8.05
CaCl <sub>2</sub> 2H <sub>2</sub> O	10.0	10.0
MgCl <sub>2</sub> 6H <sub>2</sub> O	27.9	55.5
MgSO 7H <sub>2</sub> O	27.6	0.000
NaCl	451	451
Medium headspace	N <sub>2</sub>	CH <sub>4</sub>

\* FeSO<sub>4</sub> (trace element) was replaced by FeCl (compare Widdel and Bak, 2006).



## Efficiency of the methane filter, Quepos Slide

P. Steeb et al.

Title Page

Abstract

Introduction

Conclusions

References

Tables

Figures

◀

▶

◀

▶

Back

Close

Full Screen / Esc

Printer-friendly Version

Interactive Discussion



**Table 4.** Summary of input parameters used for the model simulations and major model results. For the SO206-31 (MUC) cores, two fits are provided, since the replicate core for porewater determinations (pw-fit) exhibited a lower fluid flow and deeper SMTZ than the core used for rate determinations (hf-fit), probably as a result of high fluid flow heterogeneity at the site (see discussion).

Parameter	SO206-29 (MUC)	SO206-31 (MUC) pw-fit	SO206-31 (MUC) hf-fit	Unit	Parameter source
<b>Model parameter values</b>					
Length core	32	44	44	cm	measured
Length of simulated column	80	80	50	cm	fitted
Number of model layers	160	200	200		set
Temperature	8	8	8	°C	measured
Salinity	35	35	35	PSU	measured
Pressure	41	41	41	bar	measured
Porosity at sediment surface	0.95	0.93	0.93		measured
Porosity at the base of the sediment core	0.75	0.70	0.70		measured
Porosity at infinity sediment depth	0.74	0.70	0.70		fitted
Attenuation coef. for porosity decrease with depth	0.04	0.04	0.04	cm <sup>-1</sup>	fitted
Coefficient for tortuosity calculation	1	1	1		fitted
Burial velocity at depth	0.02	0.02	0.02	cm yr <sup>-1</sup>	fitted
Fluid flow at the sediment water interface	7	5	29	cm yr <sup>-1</sup>	fitted
Kinetic for AOM	200 000	25 000	100 000	cm mmol <sup>-1</sup> yr <sup>-1</sup>	fitted
Kinetic constant for CaCO <sub>3</sub> precipitation	0	0	0	yr <sup>-1</sup>	fitted
Density of porewater	1.03184	1.03184	1.03185	g cm <sup>-3</sup>	calculated
Density of dry solids in sediment	2.5	2.5	2.5	g cm <sup>-3</sup>	assumed
Kinetic constant for TH <sub>2</sub> S removal from porewater	0.02	0.1	0.005	mmol cm <sup>-3</sup> yr <sup>-1</sup>	fitted
Attenuation coef. for decrease in TH <sub>2</sub> S removal rate	0.07	0.6	0.05	cm <sup>-1</sup>	fitted
Non-local mixing coefficient	1.5	0	80	yr <sup>-1</sup>	fitted
Depth of irrigated layer	15	0	2	cm	fitted
Width of irrigated layer	5	0	1.5	cm	fitted
<b>Porewater concentration upper/lower boundary</b>					
Bottom water/Bottom sediment SO <sub>4</sub> <sup>2-</sup>	28.00/0.00	27.00/0.00	27.00/0.00	mmol L <sup>-1</sup>	measured
Bottom water/Bottom sediment CH <sub>4</sub>	0.00/61.00	0.00/61.00	0.00/61.00	mmol L <sup>-1</sup>	calculated*
Bottom water/Bottom sediment Cl <sup>-</sup>	558.00/380.00	548.00/320.00	548.00/320.00	mmol L <sup>-1</sup>	measured
Bottom water/Bottom sediment HCO <sub>3</sub> <sup>-</sup>	2.30/10.00	4.00/15.00	4.00/15.00	mmol L <sup>-1</sup>	measured
Bottom water/Bottom sediment TH <sub>2</sub> S	0.00/0.00	0.03/0.00	0.03/0.00	mmol L <sup>-1</sup>	measured
<b>Model Results</b>					
Methane flux at sediment bottom	12.40	9.09	45.09	mmol m <sup>-2</sup> d <sup>-1</sup>	modeled
Methane efflux at sediment water interface	0.98	0.00	3.39	mmol m <sup>-2</sup> d <sup>-1</sup>	modeled
Percentage of consumed methane	91.53	100.00	92.46	%	modeled
Anaerobic oxidation of methane	11.35	9.09	41.69	mmol m <sup>-2</sup> d <sup>-1</sup>	modeled
<b>Measured turnover rates (radiotracer techniques)</b>					
Sulfate reduction (entire sediment depth)	13.38 ± 13.61	218.90 ± 159.80	218.90 ± 159.80	mmol m <sup>-2</sup> d <sup>-1</sup>	measured
AOM (entire sediment depth)	12.87 ± 5.98	45.15 ± 11.48	45.15 ± 11.48	mmol m <sup>-2</sup> d <sup>-2</sup>	measured

\* Calculated after Tishchenko et al. (2005).

## Efficiency of the methane filter, Quepos Slide

P. Steeb et al.

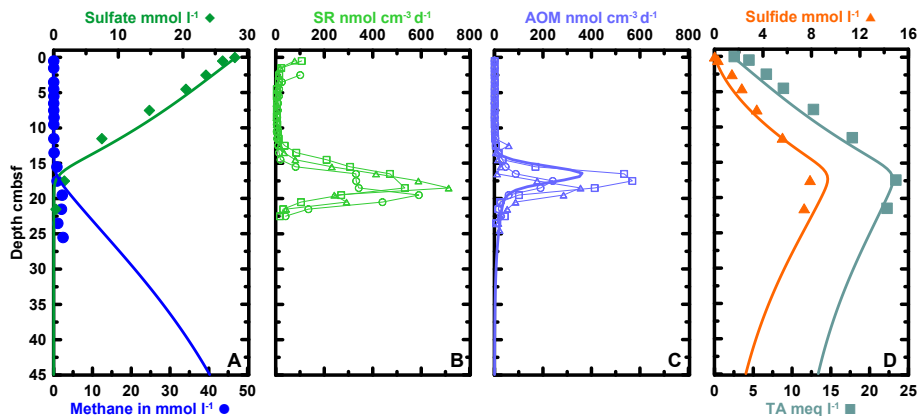


**Figure 1.** Depth profiles of measured and modeled porewater parameters as well as microbial turnover rates for SO206-29 (MUC), sampled from 402 m water depth. **(a)** measured (diamonds) and modeled (green line) sulfate concentrations as well as measured (circles) and modeled (blue line) methane concentrations, **(b)** three replicates of measured sulfate reduction rates, **(c)** three replicates of measured AOM rates (thin lines and symbols) and modeled AOM rates (thick line), **(d)** measured (triangles) and modeled sulfide concentration (orange line), measured (squares) and modeled (grey line) total alkalinity.

Title Page

Abstract

Introduction

Conclusions

References

Tables

Figures

◀

▶

◀

▶

Back

Close

Full Screen / Esc

Printer-friendly Version

Interactive Discussion



## Efficiency of the methane filter, Quepos Slide

P. Steeb et al.

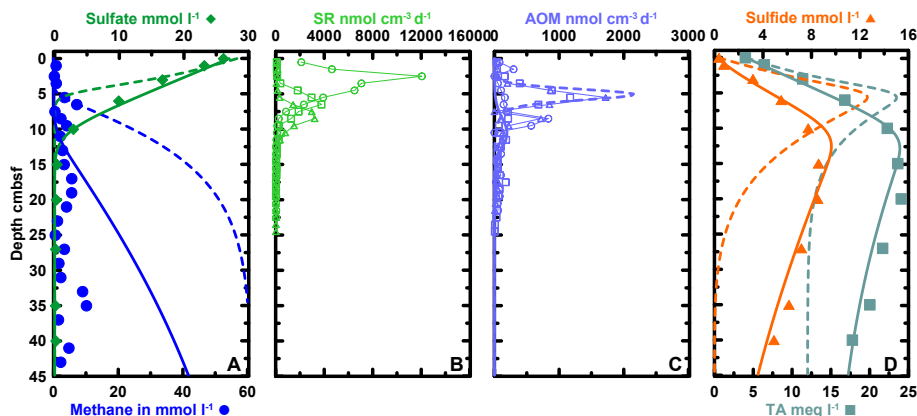


**Figure 2.** Depth profiles of measured and modeled porewater parameters as well as microbial turnover rates for SO206-31 (MUC) sampled from 401 m water depth. **(a)** Measured (diamonds) and modeled (green lines) sulfate concentrations as well as measured (circles) and modeled (blue lines) methane concentrations for the porewater fit (solid lines) and higher fluid flow fitted for the rate core (dashed lines), **(b)** three replicates of measured sulfate reduction rates, **(c)** three replicates of measured AOM rates (thin lines and symbols) and modeled AOM rates (thick lines) for the porewater fit (solid line) and higher fluid fitted for the rate core (dashed line), **(d)** measured (triangles) and modeled sulfide concentration (orange lines), measured (squares) and modeled (grey lines) total alkalinity for the porewater fit (solid lines) and higher fluid flow of the rate cores (dashed lines).

Title Page

Abstract

Introduction

Conclusions

References

Tables

Figures



Back

Close

Full Screen / Esc

Printer-friendly Version

Interactive Discussion

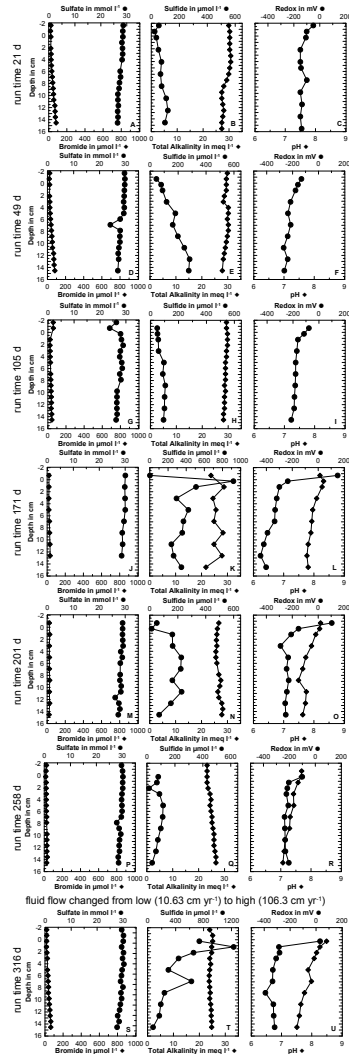


# BGD

11, 16033–16083, 2014

## Efficiency of the methane filter, Quepos Slide

P. Steeb et al.



16075

Title Page

Abstract

Introduction

Conclusions

References

Tables

Figures



Back

Close

Full Screen / Esc

Printer-friendly Version

Interactive Discussion



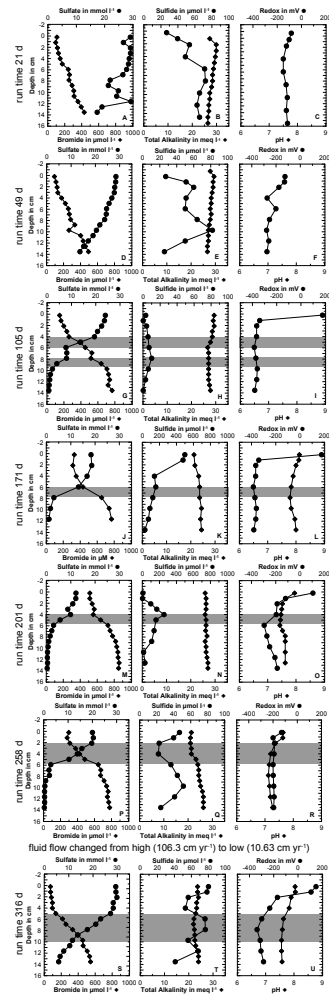


# BGD

11, 16033–16083, 2014

## Efficiency of the methane filter, Quepos Slide

P. Steeb et al.



Title Page

Abstract

Introduction

Conclusions

References

Tables

Figures



Back

Close

Full Screen / Esc

Printer-friendly Version

Interactive Discussion





## Efficiency of the methane filter, Quepos Slide

P. Steeb et al.

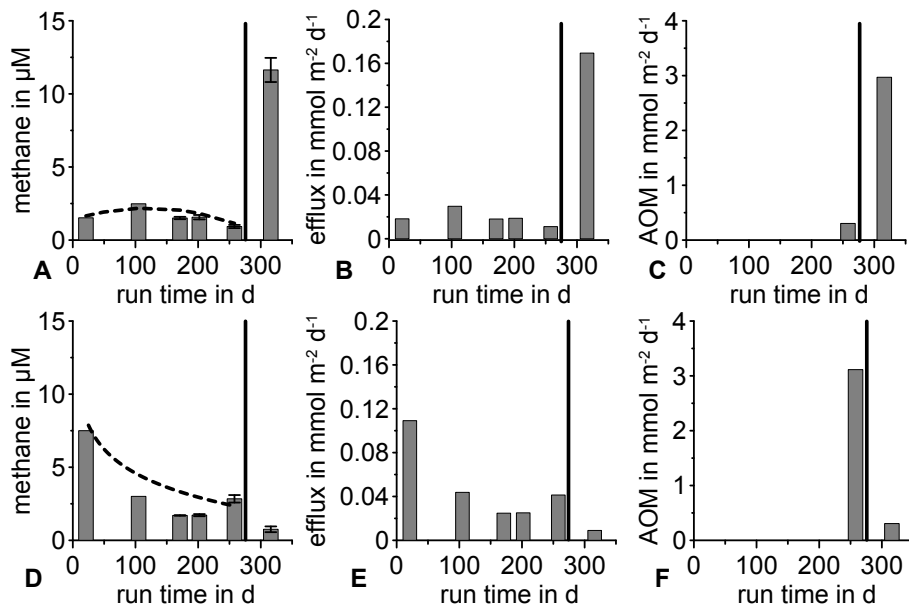


**Figure 5.** Methane concentration ( $\mu\text{mol L}^{-1}$ ) in the outflow (**a, b**), methane efflux ( $\text{mmol m}^{-2} \text{d}^{-1}$ ; **c, d**), and calculated AOM rate ( $\text{mmol m}^{-2} \text{d}^{-1}$ ; **e, f**) of the SLOT system before and after changing the fluid flow regime: (**a, c, e**) low flow regime core (LFC), and (**b, d, f**) high flow regime core (HFC) from Quepos Slide. Vertical lines mark the moment of fluid flow change (low flow  $\rightarrow$  high flow and vice versa at 258 day runtime). Error bars (**a, d**) show standard deviations of three repeated gas chromatographic measurements; the first two data points represent single measurements. Dotted lines represent the trendline (low flow regime:  $5 \times 10^{-6} \cdot t_{\text{runtime}}^2 + 0.02 t_{\text{runtime}} + 0.285$ ,  $r^2 = 0.825$ ; high flow regime:  $0.8576 \cdot \ln(t_{\text{runtime}}) - 0.8662$ ,  $r^2 = 0.987$ ) of methane concentration development until flow change.



## Efficiency of the methane filter, Quepos Slide

P. Steeb et al.

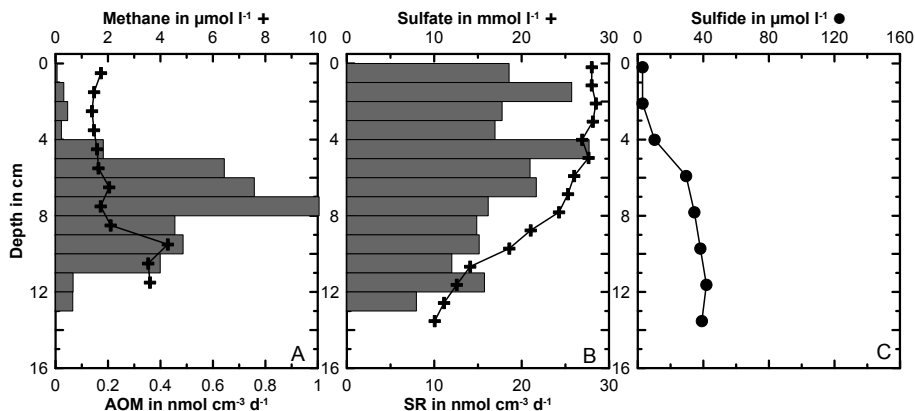


**Figure 7.** Selected concentrations and rates in the new low flow core (NLFC) after experiment termination (358 day runtime). Porewater profiles of methane (**a**, crosses), sulfate (**b**, crosses), sulfide (**c**, circles), and results of the radiotracer measurements for AOM (**a**, bars) and sulfate reduction (**b**, bars) are shown.

Title Page

Abstract

Introduction

Conclusions

References

Tables

Figures



Back

Close

Full Screen / Esc

Printer-friendly Version

Interactive Discussion



## Efficiency of the methane filter, Quepos Slide

P. Steeb et al.

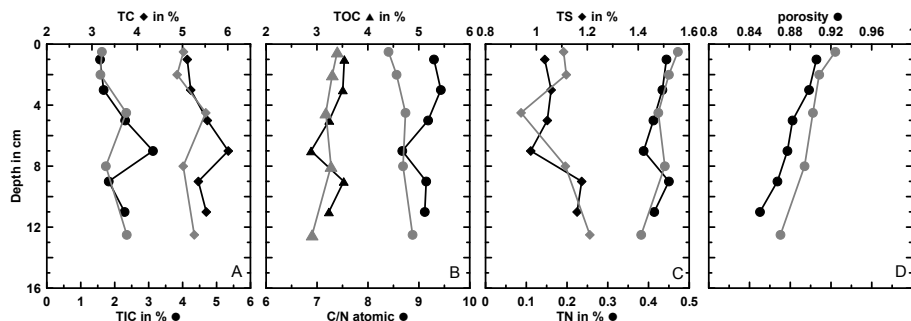


**Figure 8.** Sediment solid phase parameters measured in the sediment of the ex situ replicate SO206-31 (MUC) core (grey lines and symbols) compared to the NHFC (original LFC, black lines and symbols). Total carbon content (TC, diamonds), and total inorganic carbon content (TIC, circles) in dry wt% (a); atomic C/N ratio (circle) and total organic carbon content (TOC, triangles) in dry wt% (b); total nitrogen (TN, diamonds), total sulfur (TS, circles) in dry wt% (c); porosity of the sediment (d).

Title Page

Abstract

Introduction

Conclusions

References

Tables

Figures



Back

Close

Full Screen / Esc

Printer-friendly Version

Interactive Discussion



## Efficiency of the methane filter, Quepos Slide

P. Steeb et al.

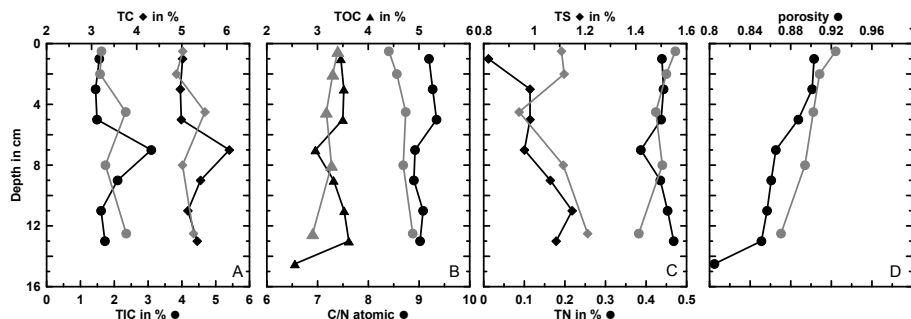


**Figure 9.** Sediment solid phase parameters measured in the sediment of the ex situ replicate of the SO206-31 (MUC) core (grey lines and symbols) compared to the NLFC (original HFC, black lines and symbols). Total carbon content (TC, diamonds), and total inorganic carbon content (TIC, circle) in dry wt% (a); atomic C/N ratio (circle) and total organic carbon content (TOC, triangles) in dry wt% (b); total nitrogen (TN, diamonds), total sulfur (TS, circles) in dry wt% (c); porosity of the sediment (d).

Title Page

Abstract

Introduction

Conclusions

References

Tables

Figures



Back

Close

Full Screen / Esc

Printer-friendly Version

Interactive Discussion

